THE JOURNAL OF PHYSICAL CHEMISTRY B

Article

Cite This: J. Phys. Chem. B 2019, 123, 5875−5891

pubs.acs.org/JPCB

Spin Probe Determination of Molecular Orientation Distribution and Rotational Mobility in Liquid Crystals: Model-Free Approach

A. Kh. Vorobiev,* A. V. Bogdanov, T. S. Yankova, and N. A. Chumakova

Department of Chemistry, Moscow State University, Leninskie Gory 1-3, Moscow 119991, Russia

Supporting Information

ABSTRACT: A model-free approach for simulation of EPR spectra of nitroxide spin probes in liquid-crystalline materials was suggested and used to obtain parameters of molecular orientation and rotational mobility. The developed method is based on experimental recording and numerical simulation of the angular dependence of EPR spectra, which is shown to be much more informative in comparison with a single EPR spectrum. Quantitative spectral simulations considering both local orientational ordering and distribution of local directors in the sample were used for discrimination of models of rotational mobility and orientational alignment. The method was applied for detailed quantitative characterization of axial, orthorhombic, and low-symmetry non-orthorhombic molecular orientation distributions. It is shown that the ordinarily used model of rotational diffusion in a mean-field potential is suitable for the description of molecular mobility and orientational ordering only for relatively low sample temperatures and low-mobility probe molecules with large sizes. In cases of high molecular mobility, the more realistic jump mechanism of molecular moves can be approximately described as quasi-librations. For ordered liquid crystals it was found that mostly the order parameters up to rank 12−14 are essential and easily determined. When well-aligned materials are described, the order parameters up to 18th rank or even higher become meaningful. Both molecular and sample biaxiality is analyzed and quantitatively characterized. The local molecular ordering and sample orientational alignment are quantitatively characterized separately.

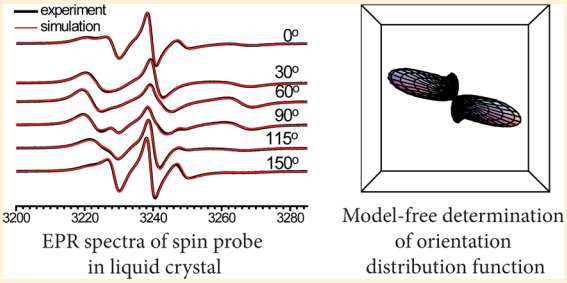

I. INTRODUCTION

The spin probe technique is widely used to characterize the molecular mobility and structure of different media. The technique consists of introducing of a small amount of a stable paramagnetic substance (the spin probe) in the studied medium and obtaining information concerning the properties of the medium by analysis of recorded electron paramagnetic resonance (EPR) spectra of the probe molecules. A variety of different systems have been studied by the spin probe method, including liquids,[1−4] glasses,[5−8] polymers,[9−16] artificial and biological membranes,[17−20] proteins,[21−23] and many others. Stable nitroxide radicals are most frequently used as spin probes. Continuous-wave EPR spectroscopy at different frequencies and pulse EPR spectroscopy of both spin probes and spin labels[24−28] provide large amounts of information. However, recording of the continuous X-band EPR spectra remains the most widespread realization of the spin probe technique because of the availability of the instrumentation and relative universality.

One of the most complicated problems in the spin probe technique is the study of anisotropic media with preferential molecular alignment such as stretched polymers, oriented fibers, membranes, and biological structures. Among these, liquid-crystalline media attract special attention because of the numerous applications and variety of structural characteristics of liquid crystals. At the same time, liquid crystals are well-defined model objects for further development of the spin probe technique. Both the molecular mobility and degree of orientational order should necessarily be characterized for adequate description of liquid-crystalline materials. The spin probe technique has been used to study liquid-crystalline media during the last 50 years. In earlier works, the characteristics of molecular order and rotational mobility were estimated directly from the positions and line widths of spectral components, respectively.[29−37] Measurements of the second-rank order parameter P_2 for ordered liquid crystals and the temperature dependence of this value have been performed using this direct treatment of EPR spectra. This approach is relatively simple, but it is limited by a set of assumptions and is inapplicable to the treatment of slow motional spectra. Therefor, numerical simulation has become at present the conventional way to analyze experimental EPR spectra. The simulation of spectra is relatively easily carried out in the cases of ordered media with negligible molecular rotational mobility.[38−43] This approach produces information concerning the shape of the molecular orientation distribution function, which is described by a set of order parameters up to 10th order without prior assumptions (i.e., a model-free method). The method was successfully applied for the study of liquid-

Received: June 7, 2019
Published: June 17, 2019

DOI: 10.1021/acs.jpcb.9b05431
J. Phys. Chem. B 2019, 123, 5875−5891

crystalline polymers[42,44] and supercooled liquid crystals,[40−47] but it does not supply information about molecular mobility specific to mesophases.

Information about molecular rotational mobility can be obtained by computer simulation of EPR spectra as well. The most known and comprehensive procedure for numerical simulation of EPR spectra of spin probes was developed in the 1980s.[48,49] Relevant software is available and widely used now.[50,51] It is based on numerical solution of the stochastic Liouville equation with a spin Hamiltonian. Large amounts of data concerning molecular rotations in different media have been obtained using this software. Most often, the obtained data are components of the rotational diffusion coefficient tensor.[52−54]

The simultaneous determination of characteristics of molecular rotations and molecular orientational order is more rarely performed. This problem was particularly important in the studies of complicated molecular orientation distributions.[55−60] The uncertainty and mutual dependence of the estimated parameters were treated in different ways. The purely empirical orientation distribution functions with adjustable parameters were used in refs 55 and 56. The prediction of EPR spectra using molecular dynamics calculations[61−65] has been suggested for substitution of the fitting of experimental spectra.

The most comprehensive and well-developed approach for simulation of experimental spectra is to use the above-mentioned software to solve the stochastic Liouville equation for rotation of the spin probe molecule in a mean-field potential describing the ordered liquid-crystalline medium. The orientation distribution function in this approach is the following:

$$\rho_{\mathrm{loc}}(\beta_l, \gamma_l) = \frac{1}{Q}\exp\left[-\frac{U(\beta_l, \gamma_l)}{k_{\mathrm{B}}T}\right] = \frac{1}{Q}\exp\left[\sum_{j,n} c_{jn} D^{j}_{0n}(\beta_l, \gamma_l)\right] \quad (1)$$

where $j, n = 2, 4$, $D^{j}_{0n}(\beta_l, \gamma_l)$ are the elements of the Wigner **D** matrix, $(0, \beta_l, \gamma_l)$ are the Euler angles transforming the local director coordinate frame to the frame of the molecular rotation axes, and $Q = \int \exp\left[-\frac{U(\beta_l, \gamma_l)}{k_{\mathrm{B}}T}\right] \sin\beta_l \, \mathrm{d}\beta_l \, \mathrm{d}\gamma_l$ is the normalization coefficient.

The local director frame in this approach is assumed to be axial, and therefore, the local potential $U(\beta_l, \gamma_l)$ and local orientation distribution in eq 1 are independent of the Euler angle α_l. Additionally, the local orientational order is supposed to be identical to the global sample orientational order. Below this approach will be called the mean-field potential (MF) method. The use of this method is described, for example, in refs 15, 59, and 66−68. Additional quantum-chemical calculations of the flexibility of the probe and hydrodynamic calculations of the mobility were proposed to diminish the number of fitting parameters.[69,70]

The determination of molecular rotational mobility and orientational alignment using the MF method demonstrates limitations, as discussed in ref 71. The most important limitations are the following:

(1) The Boltzmann expression for the mean-field potential produces correlations between values of order parameters of different ranks.[71] As a consequence, the real shape of the orientation distribution function that is defined by the full set of order parameters is not determined from EPR spectra at present.

(2) Use of the mean-field potential supposes the identity of local orientational ordering conditions for the rotating molecule and global alignment of the sample. Since this condition is obviously often violated, the available software provides the possibility to additionally define the global orientation distribution. The extreme case of the global orientation distribution is complete global disorder, which is usually described by the microscopic order and macroscopic disorder (MOMD) model. It has been proposed to describe different local and global orientational orders by local and global mean-field potentials. This possibility is used very rarely, as the local and global potentials demonstrate a strong correlation. The results presented in refs 15 and 58 demonstrate that the local and global potentials cannot be reliably distinguished.

(3) Only the Brownian mechanism is used for molecular rotations in liquid crystals. The mechanisms of jumps and free rotation cannot be used for ordered media because of huge computational difficulties.

(4) The simultaneous determination of the rotation and orientation parameters requires a large number of fitting parameters in the course of simulation of the EPR spectra. The parameters often demonstrate correlation, which complicates obtaining reliable information. This trouble is particularly serious when desirable values are extracted from one EPR spectrum. This is the reason to search for independent sources of experimental data and diminish the set of used parameters.

During the numerical simulations of EPR spectra in liquid crystals, the simulated spectra often demonstrate only approximate similarity to the experimental ones, that is, the deviation of the calculated spectra from the experimental ones exceed the experimental uncertainty. It is possible that the mentioned limitations are responsible for such deviations. Overcoming these limitations and obtaining more reliable and meaningful results by the spin probe technique for ordered media is the purpose of the present contribution. We have used the following approaches. For more reliable characterization of the orientation distribution, we use a combination of the mean-field and model-free approaches. The mean-field potential with the Boltzmann distribution function is retained to describe the local conditions for the rotating spin probe molecule. The distribution of these local directions in the sample is described by expansion in a series of elements of the Wigner **D** matrix:

$$\rho_{\mathrm{sam}}(\alpha_s, \beta_s, 0) = \sum_{j,m} \frac{2j+1}{8\pi^2} \langle D^{j}_{m0}{}^{*} \rangle_{\mathrm{sam}} D^{j}_{m0}(\alpha_s, \beta_s, 0) \quad (2)$$

where $(\alpha_s, \beta_s, \gamma_s)$ are the Euler angles transforming the sample frame to the local director frame.

Convolution of the molecular distribution defined by eq 1 and the distribution shown in eq 2 produces the global orientation distribution of probe molecules in the sample frame:

$$\rho(\alpha, \beta, \gamma) = \sum_{j,m,n} \frac{2j+1}{8\pi^2} \langle D^{j}_{mn}{}^{*} \rangle D^{j}_{mn}(\alpha, \beta, \gamma) \quad (3)$$

DOI: 10.1021/acs.jpcb.9b05431
J. Phys. Chem. B 2019, 123, 5875−5891

where (α, β, γ) are the Euler angles connecting the molecular and sample frames and $P_{jmn} \equiv \langle D^j_{mn}{}^* \rangle$ are the orientational order parameters.

The coefficients of the series in eq 3 define the independent order parameters, which allow the description of any orientation distribution function. Below this approach will be called the orientation distribution function (ODF) method.

We intended to use a more realistic molecular rotation mechanism in the course of EPR spectra simulation as well. The well-founded model of molecular rotations is the slow relaxed local structure (SRLS) model,[72,73] in which the local cage potential persists for a mean time that is much longer than the rotational correlation time of the individual molecule rotating in that cage. Unfortunately, the calculations within this model for well-ordered liquid crystals are too complicated and time-consuming. Therefore, we used the simplified SRLS model, which supposes high-frequency intracage rotations and slower rotations related to cage reorganization. We describe the high-frequency rotation moves using a libration model in which the partial averaging of magnetic parameters is calculated explicitly. The stochastic Liouville equation in this case describes the slower cage reorganization process. The model of averaging libration was successfully used earlier to describe the EPR spectra of spin probes in glassy and polymer media[5,14,20,74−76] as well as for spin labels attached to large molecules.[53,77] As the high-frequency rotations in liquid-crystalline media are not harmonic small-angle moves, we use the term "quasi-libration".

The use of more complicated models with a greater number of parameters requires special efforts to obtain reliable results. The enhancement of the informativity of the spin probe technique in the case of ordered media is made possible by numerical simulation of the detailed angular dependence of the EPR spectra. This approach is easily realized in the case of smectic liquid crystals, which do not change their alignment in the magnetic field of the X-band EPR spectrometer. On the contrary, nematic liquid crystals are rapidly reoriented in the EPR magnetic field, and therefore, the angular dependence of the spectrum of a bulk nematic sample cannot be recorded. To overcome this limitation, we used thin quartz cells, where the oriented nematic mesophase is anchored to the solid cell walls and loses the ability to reorient in the magnetic field. The joint numerical simulation of 10−20 different spectra of angular dependence significantly improves the reliability of the results and allows determination of a larger number of fitting parameters. The strict requirement of coincidence of the calculated and experimental spectra within the experimental uncertainty additionally improves the reliability of the method.

II. COMPUTATIONAL DETAILS

A few coordinate frames are used in the present work: the sample frame, the local director frame, the molecular **g** tensor frame, and the molecular orientation frame, which coincides with molecular rotation frame. The Euler angles $(0, \beta_D, \gamma_D)$ connect the **g** tensor molecular frame with the molecular orientation frame. The Euler angles $(\alpha_s, \beta_s, \gamma_s)$ transform the sample frame to the local director frame. The Euler angles $(0, \beta_l, \gamma_l)$ connect the local director frame with the molecular frame. The Euler angles (α, β, γ) transform the sample frame to the molecular frame. Figure S1 in the Supporting Information illustrates these transformations.

Numerical simulation of the EPR spectra of unordered samples under rigid-limit conditions (77−100 K) was performed using the program described in ref 78. Values of the magnetic parameters of radicals (i.e., the components of the **g** tensor and the hyperfine interaction (hfi) tensor) were determined in the course of these simulations. The obtained values and typical results of the rigid-limit simulations are presented in section ESI.II in the Supporting Information. The obtained magnetic parameters were used in the course of simulation of spectra recorded for liquid-crystalline mesophases. The stochastic Liouville equation was solved for the latter simulations. The software used in the present work was an elaborated version of the well-known program described in ref 50. The program was modified to use the averaging of magnetic parameters with quasi-librations and implement the orientation distribution described by eq 3. In the program, the local orientation distribution in the cage of the medium is defined by the mean-field potential (eq 1) with coefficients c_{20}, c_{22}, c_{40}, c_{42}, and c_{44}. The local order parameters were calculated as follows:

$$\mathrm{Ploc}_{j0n} \equiv \langle D^j_{0n}{}^* \rangle = \frac{\int D^j_{0n}{}^*(\Omega_l) \exp\left(-\frac{U(\beta_l,\gamma_l)}{k_B T}\right) \mathrm{d}\Omega_l}{\int \exp\left(-\frac{U(\beta_l,\gamma_l)}{k_B T}\right) \mathrm{d}\Omega_l} \quad (4)$$

where $\Omega_l \equiv (0, \beta_l, \gamma_l)$ is the set of Euler angles connecting the local director and molecular frames.

The limitation of this approach is the axial symmetry of the local orientation distribution of the probe molecules. This limitation indicated by the value of zero for the second index in the mean-field potential coefficients. As a result, this approach, strictly speaking, cannot be used in the case of locally biaxial smectic C (SmC) mesophases.

An orientation distribution of the local axial director in the sample frame is defined by the coefficients in eq 2. The order parameters for this distribution are

$$\mathrm{Psam}_{jm0} \equiv \langle D^j_{m0}{}^* \rangle \quad (5)$$

The rank of the expansion in eq 2 was determined in the course of simulation of spectra. For this purpose, the simulation was performed several times, sequentially increasing the expansion rank until a further increase in the expansion rank ceased to improve the quality of the simulation of experimental spectra. Details of the determination of the necessary rank and experimental examples are presented in ESI.III. The third index in eq 5 is equal to zero as a result of the local axial symmetry of the potential. The set of determined order parameters must satisfy the physically reasonable condition of non-negativity of the molecular distribution function. To fulfill this condition, in some cases we used a penalty function that restricted the minimization procedure to the range of non-negativity of the orientation distribution.

The convolution of these two distribution functions describes the experimentally observed orientation distribution of probe molecules. The global order parameters characterizing the experimental EPR spectra are calculated in the considered case as follows (see ESI.I):

$$P_{jmn} = \mathrm{Psam}_{jm0} \cdot \mathrm{Ploc}_{j0n} \quad (6)$$

The described approach includes as a particular case the MOMD model meant for description of spectra for unordered samples.

DOI: 10.1021/acs.jpcb.9b05431
J. Phys. Chem. B 2019, 123, 5875−5891

The averaging of the magnetic parameters of the paramagnetic probe by high-frequency librations can be described by different expressions depending on the model of the angular displacement.[5,11,20,74,76,77] All of these characteristics are only semiquantitative.[78] In the present work, we used the following averaging expressions for quasi-librations around three magnetic axes simultaneously[11] (the derivation is presented in ESI.IV):

$$\langle A_x\rangle = A_x + 0.5(A_z - A_x)(1 - P_y) + 0.5(A_y - A_x)(1 - P_z)$$
$$\langle A_y\rangle = A_y + 0.5(A_z - A_y)(1 - P_x) + 0.5(A_x - A_y)(1 - P_z)$$
$$\langle A_z\rangle = A_z + 0.5(A_x - A_z)(1 - P_y) + 0.5(A_y - A_z)(1 - P_x) \quad (7)$$

where $P_x = (\sin L_x \cos L_x)/L_x$, $P_y = (\sin L_y \cos L_y)/L_y$, and $P_z = (\sin L_z \cos L_z)/L_z$; $\langle A_x\rangle$, $\langle A_y\rangle$, $\langle A_z\rangle$, A_x, A_y, and A_z are averaged and intrinsic hyperfine constants, respectively; and L_x, L_y, and L_z are half-amplitudes of the motion around the x, y, and z magnetic axes, respectively. The expressions in eq 7 describe the averaging of the hfi tensor components. The averaging of the **g** tensor components is described by analogous expressions.

The presented approach distinguishes the local fast angular displacements described by the quasi-libration amplitudes L_x, L_y, and L_z and the slower reorganization of the liquid-crystalline cage described by the rotational diffusion components D_x, D_y, and D_z. The orientation of the diffusion axes relative to the main axes of the **g** tensor is described by the Euler angles $(\alpha_D, \beta_D, \gamma_D)$.

In all cases, fitting of the experimental spectra with variation of parameters was performed using the nonlinear least-squares fitting procedure NL2SOL.[79] Unweighted differences between points in the experimental and simulated spectra were used as minimized residuals r_i. The resulting discrepancy was calculated as follows:

$$D = \sum_i \frac{r_i^2}{n} \quad (8)$$

where n is the total number of calculated points.

The values of the discrepancy were calculated for spectra that were normalized on double integrals. The covariance matrix calculated in the final point of fitting was used for detection of interdependent parameters. This matrix can also be used for estimation of standard deviations and confidence ranges for the obtained values.[79,80] However, repeated experiments and simulations showed that both t statistics and χ^2 statistics produce underestimated values of the uncertainty level for the determined parameters. Therefore, the uncertainties for parameters under consideration were estimated in the present work by direct calculations of the dependence of the discrepancy on this parameter near the point of minimum. The procedure for determining errors in the order parameters is discussed in detail in ESI.V. Typical uncertainties estimated using this procedure are presented in Table 1.

The additional EPR components generated by the natural content of the ^{13}C isotope were observed in experimental spectra in the cases of relatively large rotational mobility. These components were simulated by addition of corresponding paramagnetic centers with supplementary hyperfine splittings. The probe molecules containing ^{13}C were found to demonstrate additional hyperfine coupling in the range 5−6 G and a content of about 6%.

Table 1. Typical Uncertainty Levels for the Determined Parameters

parameter	confidence range and correlations
Gaussian line width (G)	(0−2.5) ± 0.1
Lorentzian line widths LorX, LorY, LorZ (G)	(0−2.5) ± 0.3; can correlate with D_x, D_z
diffusion rotation tensor D_x, D_y, D_z (s^{-1})[a]	∼(2 ± 1) × 10^7, ∼(5 ± 1) × 10^8; can correlate with c_{20}, c_{22}, Lorentzian line widths, and libration amplitudes
diffusion axis tilt angles β_D, γ_D (deg)	β_D, γ_D ± 3
libration amplitudes L_x, L_y, L_z (deg)	L ± 5
local potential coefficients c_{jn}	±1−5; c_{20} strongly correlates with other c_{jn}
global order parameters P_{jmn}	P_{j00} ± (0.01−0.02); P_{jm0} ± (0.01−0.05)

[a]The uncertainty depends on the order of magnitude of the diffusion coefficient value. Typical uncertainties for different values are presented.

III. EXPERIMENTAL DETAILS

III.1. Substances. The liquid crystals 4-*n*-pentyl-4′-cyanobiphenyl (5CB) and 4-*n*-octyl-4′-cyanobiphenyl (8CB) were obtained from Merck and used without purification. The liquid crystals *p*-hexyloxyphenyl *p*-decyloxybenzoate (HOPDOB) and *p*-hexyloxyphenyl *p*-octyloxybenzoate (HOPOOB) were produced by RIAP (Kiev, Ukraine) and purified by recrystallization from ethyl acetate. The liquid crystal *N*-decyloxybenzylidene-*p*-toluidine (H59) was obtained from REACHEM and purified by recrystallization from ethanol. The structures of all of the liquid crystals used are presented in Figure 1.

The used liquid crystals exhibited sharp phase transitions with temperatures consistent with literature data, as shown in Table 2.

The stable nitroxide radicals presented in Figure 2 were used as spin probes. Spin-labeled cholestane (CSL) was purchased from Sigma-Aldrich. Radicals C4 and C11 were synthesized by the group of Prof. R. Tamura (Kyoto University, Japan) using the procedures described in refs 87 and 88. Radicals A1,[89] A3,[90] A4,[91] and A5[92] were synthesized by the group of Prof. S. Bottle (Queensland University, Australia).

III.2. Sample Preparation. Radicals were dissolved in the liquid crystals at temperatures exceeding the clearing points of the materials. The concentrations of radicals were about 1 × 10^{-3} M, and the average distance between paramagnetic molecules was about 100 Å. The broadening of spectral lines did not exceed 0.05 G and really did not appear in the EPR spectra.

Liquid crystals containing spin probes were placed in quartz ampules with an inner diameter of 4 mm, and the heights of the samples were 3−8 mm. The samples were freed from oxygen by evacuation at 10^{-3} Torr for 2−3 h at the temperatures of the mesophases. However, oxygen broadening was found to be negligible in the cases of liquid crystal mesophases and it did not significantly influence the obtained results.

DOI: 10.1021/acs.jpcb.9b05431
J. Phys. Chem. B 2019, 123, 5875−5891

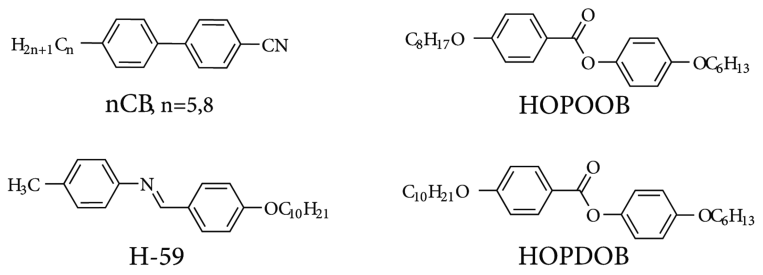

Figure 1. Chemical structures of the liquid crystals.

Table 2. Phase Behavior of the Liquid Crystals Used

liquid crystal	phase behavior	ref(s)
5CB	Cr 296 N 308 Iso	81
8CB	Cr 294 SmA 306 N 313 Iso	82
HOPOOB	Cr 329 SmC 339 N 362 Iso	83, 84
HOPDOB	Cr 335 SmC 351 SmA 356 N 362 Iso	85
H59	Cr [337 SmB][a] 343 SmA 351 N 352 Iso	86

[a]Observed only on cooling.

Preparation of the macroscopically disordered liquid crystals was performed by cooling the samples from isotropic liquids to the temperatures of the mesophases in the absence of a magnetic field. For preparation of aligned smectic liquid crystals in bulk samples, the samples in the nematic mesophase were exposed to the magnetic field of the EPR spectrometer (6000 G) for 5 min. Oriented nematic samples were further cooled in the magnetic field to the temperatures of the smectic mesophases.

The angular dependence of spectra in oriented nematic mesophases cannot be recorded in bulk samples because nematic liquid crystals rapidly reorient under the influence of the magnetic field of the EPR spectrometer. To record angular dependences of the spectra for nematics, we used cells with a thickness of 11 μm. Two quartz plates composing the cell were treated for 24 h with $(CH_3)_2Cl_2Si$ vapor to produce a hydrophobic surface.[93,94] This anchoring surface causes the homeotropic orientation of liquid crystals. The thicknesses of the cell were settled by calibrated glass rod spacers. Earlier,[55] Luckhurst calculated the threshold thickness of the 5CB liquid crystal layer that is not influenced by the magnetic field of the EPR spectrometer. The known value of the bend elastic constant was used for this calculation. The threshold thickness was estimated to be about 20 μm.[55]

In the present work, we verified this prediction experimentally. Fréedericksz-type experiments were performed in the setup shown in Figure 3a. The magnetic field dependencies of the transmittance of the LC cell in the crossed polarizers for nematic 8CB are presented in Figure 3b. The figure demonstrates the threshold magnetic fields for 11 and 25 μm cells. It can be seen that the value of the threshold field

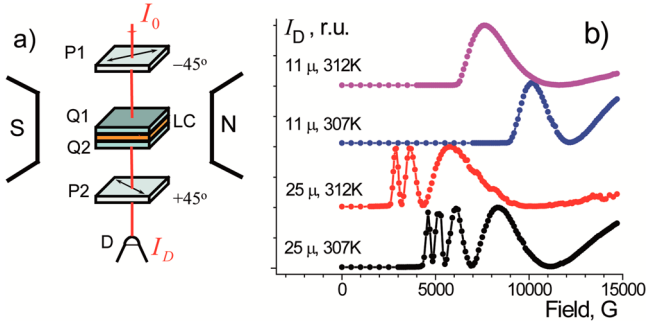

Figure 3. (a) Setup of the magnetic Fréedericksz experiment. I_0 and I_D are the intensities of the initial and detected laser beams, respectively, P1 and P2 are crossed polarizers, Q1 and Q2 are quartz plates, LC is the liquid crystal, D is the photodiode, and N and S denote the magnetic field directed at an angle of 45° with respect to the polarization of the beam. (b) Photocurrent of the detector vs magnetic field for sample 8CB in 25 and 11 μm cells. The dependencies have been shifted vertically for clarity.

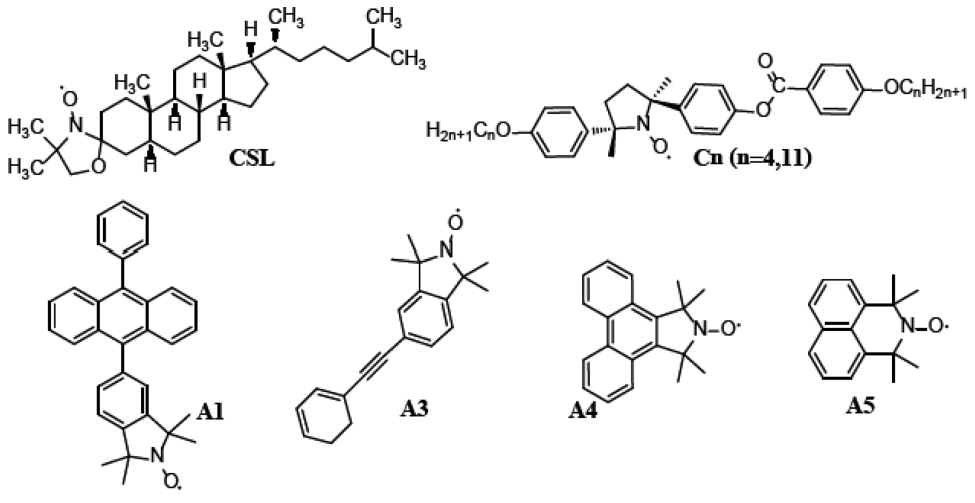

Figure 2. Stable nitroxide radicals used as spin probes.

DOI: 10.1021/acs.jpcb.9b05431
J. Phys. Chem. B 2019, 123, 5875−5891

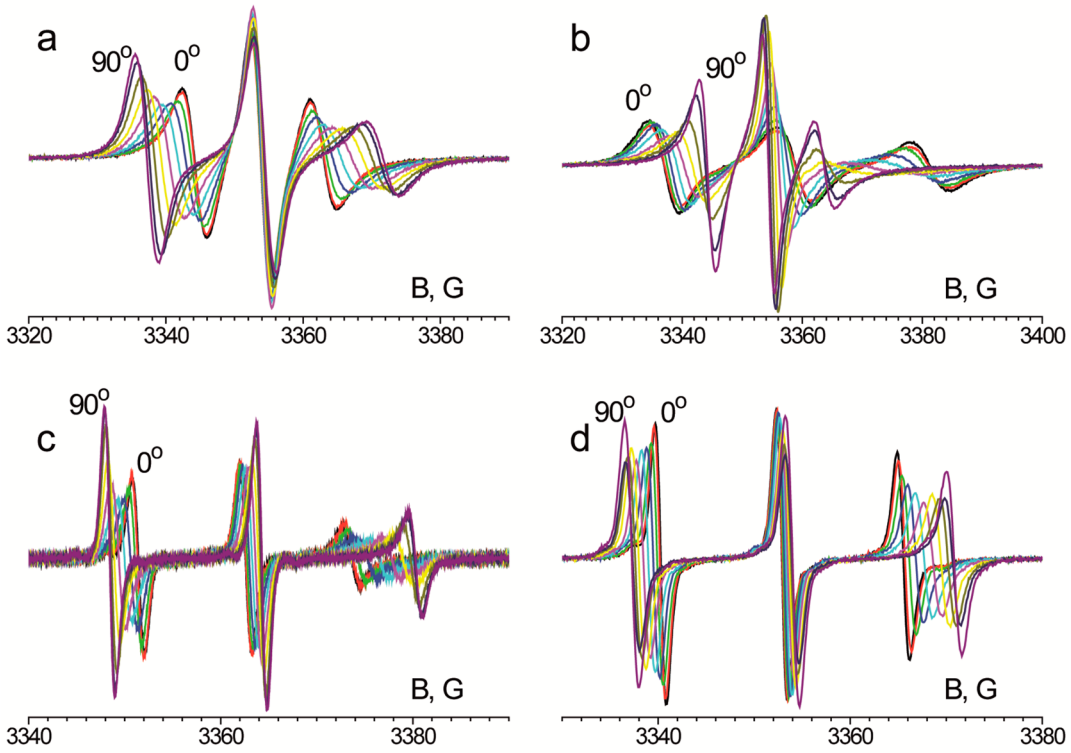

Figure 4. Experimental angular dependences of EPR spectra: (a) CSL/5CB, 303 K (N); (b) C4/8CB, 299 K (SmA); (c) A3/HOPDOB, 353 K (SmA); (d) A5/HOPOOB, 355 K (N). For clarity, only 10 spectra out of 19 are presented for every angular dependence.

depends on the temperature of the mesophase. The obtained data confirmed the mentioned prediction and demonstrated the possibility of recording X-band EPR angular dependences using the 11 μm cells, as the threshold field for this sample was significantly higher than the magnetic field of the X-band EPR spectrum.

III.3. Recording of EPR Spectra. EPR spectra were recorded using a Bruker EMX500 Plus spectrometer. For investigations of macroscopically aligned liquid crystals, series of 15−20 spectra were recorded at different orientations of a sample relative to the direction of the magnetic field. In the course of such experiments, the sample was turned around the axis perpendicular to the liquid crystal director using an automatic goniometer with an accuracy of 0.5°. Nineteen spectra were usually recorded: from 0° to 90° and from 95° to 175° with 10° steps. The coincidence of spectra at 0° and 180° was verified. A variable-temperature unit from Bruker was used for recording of EPR spectra. The Bruker Dewar tube for the temperature unit was modified to avoid vertical and horizontal temperature gradients specific to the source setup. The accuracy of the sample temperature was ±0.5°. It was verified that spectra of angular dependence were invariant over several hours.

IV. RESULTS AND DISCUSSION

IV.1. Angular Dependence of the EPR Spectra of Nitroxides in Ordered Liquid Crystals and Their Numerical Simulations. Typical angular dependences of the EPR spectra of the nitroxide probes in well-oriented liquid crystals are presented in Figure 4. The EPR spectra presented in Figure 4 demonstrate strong angular dependence. This indicates that all of the spin probes used, both small and large, are incorporated into the liquid-crystalline structure and therefore reflect the orientational order of medium. As can be seen, the spectra of small probe molecules in high-temperature mesophases are considerably narrower than the spectra of probes with large molecular sizes at lower temperatures. Obviously, this is the result of larger molecular mobility of small molecules. This circumstance may lead to even more informativity of the small paramagnetic probes compared with traditional larger probes such as spin-labeled cholestane (CSL).

The treatment of the spectra for the studied systems consisted of the joint numerical simulation of all spectra of the angular dependence. The problems solved by spectra simulation were (i) determination of the model of orientational order and (ii) clarification of the molecular rotational mechanism suitable for description of the EPR spectra as well as (iii) estimation of the physical characteristics of the medium. Typical results of both successful and unsuccessful simulations of angular dependences are illustrated in Figure 5. Only four spectra for every system are presented in the figure. The results of the simulations for all of the studied systems are listed in Table 3.

The simulations presented in Figure 5a,b are characterized by agreement between the calculated and experimental spectra within the spectral noise. Such simulations are marked in Table 3 as "quantitative simulations". The calculated spectra shown in Figure 5c,d demonstrate small deviations from the experimental ones with respect to amplitudes and widths of spectral components. Nevertheless, in Table 3 we qualify such simulations as satisfactory taking into account experimental errors, such as small temperature deviations in the course of recording the angular dependence. The simulations marked in Table 3 as "failed" are the best possible descriptions of the corresponding spectra, but in these cases the positions and

DOI: 10.1021/acs.jpcb.9b05431
J. Phys. Chem. B 2019, 123, 5875−5891

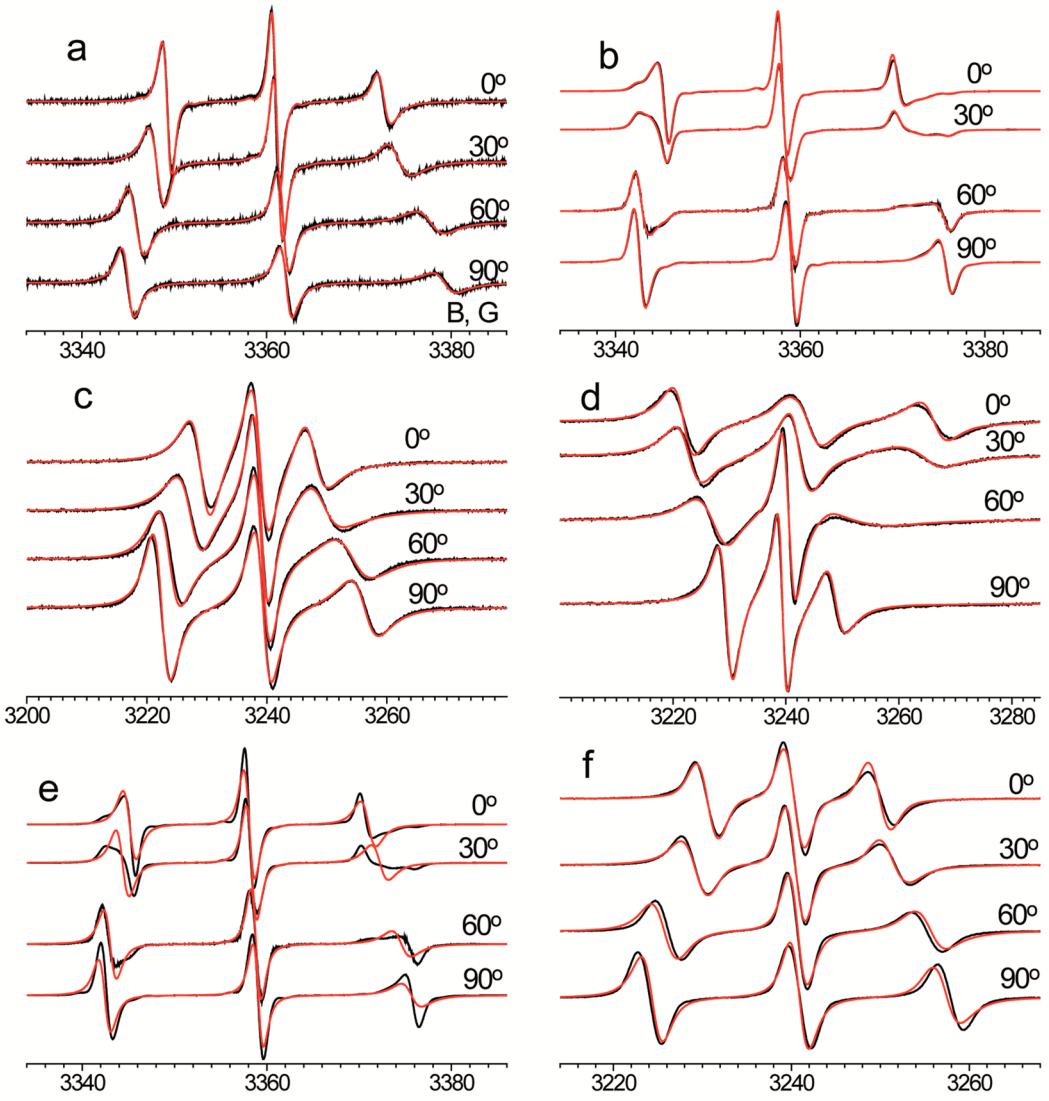

Figure 5. Examples of (a, b) quantitative, (c, d) satisfactory, and (e, f) failed simulations of experimental angular dependences: (a) A5/8CB (N, 308 K, ODF model + librations); (b) A5/H59 (SmA, 347 K, ODF model + librations); (c) CSL/5CB (N, 305 K, MF model); (d) C4/8CB (SmA, 299 K, ODF model); (e) A5/H59 (SmA, 347 K, MF model); (f) CSL/HOPDOB (N, 359 K, ODF model). Black lines are experimental spectra, and red lines are results of simulations.

shape of calculated spectral components differ appreciably from the experimental ones. We suppose that the quantitative data obtained by such simulations may be unreliable.

The assessment of the obtained simulations was performed not only by the degree of coincidence of the experimental and calculated spectra but also by the physical meaning of the obtained values. In cases where the optimal values of the parameters achieved in the course of the minimization procedure have clear physical meaning, the simulation is marked in Table 3 as demonstrating "rational" parameters. The conclusion "baseless" in the last column of Table 3 means that the obtained values of the parameters contradict known properties of liquid crystals or probe molecules. In Table 3, the studied systems are divided into a few groups on the basis of the described two criteria.

Group I contains large probe molecules in well-aligned liquid crystals (systems 1−4). The EPR spectra for these systems can be simulated using both the MF and ODF models with approximately equal quality. The parameters of rotational mobility and orientational order take approximately the same values in the course of both types of simulation. These values will be discussed below in more detail (sections IV.2 and IV.3). One can conclude that the diffusion mechanism of rotational mobility is appropriate for these systems.

The nitroxide probes with smaller molecular sizes (systems 6−12) compose group III in Table 3. The angular dependence of the EPR spectra for these systems cannot be described using the rotational diffusion mechanism in the frame of both the MF and ODF models. The criteria for a good simulation, namely, agreement of the experimental spectra with the calculated ones and the physical sense of the parameters, are violated in these simulations. An example of an unsatisfactory simulation is presented in Figure 5e. Correct simulations of the spectra for these systems can be achieved only using the molecular rotation mechanism combining relatively slow rotational diffusion and quasi-librations with frequency averaging. Both the MF and ODF modes with the combined mechanism produce satisfactory simulations. At the same time,

DOI: 10.1021/acs.jpcb.9b05431
J. Phys. Chem. B 2019, 123, 5875−5891

Table 3. Models Suitable for Simulation of the Angular Dependence of EPR Spectra of Nitroxide Probes in Liquid-Crystalline Media

system	probe/LC	sample	model	libr.	D_{par}/D_{perp}	N_{var}[a]	discr.	simulation	parameters
			I. Rotational Diffusion in Aligned Liquid Crystals: Successful Simulations						
1	CSL/5CB, 305 K (N)	layer	MF	no	15.4	9	3.0×10^{-7}	satisfactory	rational
			ODF	no	9.6	14	2.7×10^{-7}	satisfactory	rational
2	C4/8CB, 299 K (SmA)	layer	MF	no	401	13	1.5×10^{-7}	satisfactory	rational
			ODF	no	129	16	1.4×10^{-7}	satisfactory	rational
3	C11/8CB, 300 K (SmA)	bulk	MF	no	21.5	10	1.4×10^{-7}	satisfactory	rational
			ODF	no	372	13	2.6×10^{-7}	satisfactory	rational
4	CSL/HOPDOB, 354 K (SmA)	layer	MF	no	27.2	10	1.8×10^{-6}	satisfactory	rational
			ODF	no	1.5	25	2.5×10^{-6}	satisfactory	rational
			II. Rotational Diffusion in Aligned Liquid Crystals: Failed Simulations						
5	CSL/HOPDOB, 359 K (N)	layer	MF	yes	44	14	2.4×10^{-6}	failed	baseless
			ODF	yes	21	22	2.6×10^{-6}	failed	baseless
			III. Rotational Diffusion and High-Frequency Quasi-Librations in Aligned Liquid Crystals						
6	A3/HOPDOB, 353 K (SmA)	bulk	MF	yes	7.1	14	2.0×10^{-5}	failed	rational
			ODF	yes	4.0	23	5.8×10^{-6}	satisfactory	rational
7	A4/HOPDOB, 353 K (SmA)	bulk	MF	yes	>2000	14	1.1×10^{-5}	failed	baseless
			ODF	yes	1.5	48[c]	3.8×10^{-6}	satisfactory	rational
8	A5/HOPDOB, 353 K (SmA)	layer	MF	yes	3.2	10	5.3×10^{-5}	satisfactory	baseless
			ODF	yes	1.0[b]	62[c]	5.3×10^{-5}	satisfactory	rational
9	A5/HOPOOB, 355 K (N)	layer	MF	yes	423	11	2.6×10^{-6}	quantitative	baseless
			ODF	yes	1.0[b]	17	3.3×10^{-6}	satisfactory	rational
10	A5/H59, 347 K (SmA)	bulk	MF	yes	>2000	10	8.9×10^{-6}	satisfactory	baseless
			ODF	yes	1.0[b]	13	4.2×10^{-6}	quantitative	rational
11	A5/H59, 340 K (SmB)	bulk	MF	yes	>2000	10	8.2×10^{-6}	satisfactory	baseless
			ODF	yes	1.0[b]	13	3.7×10^{-6}	quantitative	rational
12	A5/8CB, 308 K (N)	layer	MF	yes	51	11	5.6×10^{-6}	satisfactory	baseless
			ODF	yes	1.0[b]	18	4.2×10^{-6}	quantitative	rational
			IV. Complicated Orientation Distributions						
13	A5/8CB, 303 K (SmA)	axial, layer	MF	no	5.5	10	2.0×10^{-6}	quantitative	baseless
			ODF	no	1.5	24	3.1×10^{-6}	satisfactory	rational
14	A1/8CB, 301 K (SmA)	axial, bulk	MF	no	2.6	12	2.9×10^{-8}	satisfactory	rational
			ODF	no	3.7	18	2.1×10^{-8}	satisfactory	rational
15	C4/HOPDOB, 354 K (SmA)[e]	axial, bulk	ODF[d]	yes	89.0	30	9.9×10^{-7}	satisfactory	rational
				no	>1000				
16	A5/HOPDOB, 353 K (SmA)[e]	orthorhombic, bulk	ODF	yes	1.0[e]	63	6.2×10^{-6}	satisfactory	rational
17	C4/8CB, 297 K[e] (SmA distorted by magnetic field; Figures 9 and 10)	non-orthorhombic, layer	ODF	no	50.3	63	4.6×10^{-8}	satisfactory	rational

[a]The number of parameters does not include the values describing the amplitude and field position of the spectrum as a whole or the parameters of ^{13}C-containing admixtures. [b]The anisotropy of rotation does not matter within the error of the simulation. [c]The small macroscopic biaxiality of the sample was taken into account with a corresponding increase in the number of variables. [d]The calculated spectra are the sums of spectra for two probe molecules with different rotational mobilities. [e]The simulation of the system using the MF model failed.

even including this mechanism, the MF model failed to satisfy the criterion of physical sense. In particular, the large anisotropy of rotational mobility obtained within the MF model simulation is incredible for compact probe A5. In addition, such simulations as a rule gave unreasonably small values of the order parameter P_{200} (~0.25) that are irrelevant for well-ordered liquid crystals. One can conclude that the ODF model is more adequate in these cases. Optimal values of the variables will be discussed below in section IV.3.

One can notice in Table 3 that the discrepancies between the experimental and calculated spectra in the cases of large and small probes differ by more than order of magnitude. Really, this difference does not reflect the quality of the simulation but is the result of considerably narrower EPR spectra in the case of small radicals. The amplitudes of the spectral components and the value of the discrepancy hereupon is noticeably larger. The simulations of the spectra for small radical probes also reveal the larger sensitivity of these probes to the orientational order of the sample. This feature was observed in the cases of samples 7 and 8 in Table 3. It was found that the experimental spectra of these systems are sensitive to very small biaxial distortions of the orientation alignment. The distortions are induced by inaccuracies in the experiment such as small temperature gradients and defects of the anchoring surface. The biaxial distortion corresponds to very small values of sample biaxial parameters, which will be discussed below. Nevertheless, they lead to noticeable changes in the spectra and should be considered in the course of numerical simulations.

DOI: 10.1021/acs.jpcb.9b05431
J. Phys. Chem. B 2019, 123, 5875−5891

Thus, the systems in group I are described within the rotational diffusion model. The spin probes in group III demonstrate additionally the averaged quasi-librations, which can be attributed to local rotational jumps with high frequency. This feature is the result of the smaller size of the probe molecules and the higher temperature of the mesophases for these cases. System 5 in Table 3 corresponds to an intermediate case. The spectra in this case (CSL/HOPDOB) cannot be described quantitatively by either approach. The molecular mobility in the nematic HOPDOB is relatively high, but the size of the probe CSL is large. We believe that the rotational jumps of CSL under these conditions occur with insufficient frequency to use the simplified libration model. A rough description of the spectra can be achieved within the quasi-libration model, but the amplitudes of the librations around all three axes become incredibly large. An explicit model of low-frequency jumps in the local potential should be considered in this case. Unfortunately, at present there is no appropriate method for such calculations.

The fourth group of studied systems collects the cases of complicated orientation distributions. The real orientational ordering is the convolution of the local distribution of probe molecules relative to the local director with the macroscopic distribution of the directors in the sample. The experiment shows that both distributions can be imperfect. Systems 13 and 14 are examples of dual orientation of the probe molecules when two different orientations of probes relative to the LC director are possible. This possibility is apparently the result of different positions of the probe in the liquid-crystalline structure. In both systems it diminishes the observed angular dependence of the EPR spectra. The two positions of the probe molecules are seen in the obtained orientation distribution function, which will be discussed below. It should be noted that systems 12 and 13 differ only by temperature (5 K) and type of mesophase (nematic and smectic A, correspondingly). Nevertheless, in the smectic phase two distinct orientations of the probe are observed, while they are not seen in the nematic phase. This means that the frequency of jumps between different positions in the nematic phase is sufficiently high to average these two states on the EPR time scale. Systems 14 and 15 are examples of systems in which the different positions of the probe molecules are almost independent, as the frequency of transitions between the positions is too low. Systems 16 and 17 are examples of distortion of the sample orientation distribution under two competitive orienting factors.

One can try to study SmC mesophases by the methods described above. However, the experiments showed that the description of the angular dependences for SmC is markedly worse in comparison with that for the SmA phases. We believe that the reason for this difference is the microscopic nonaxiality of the SmC phase, which is not described by known simulation methods.

The important issue for spectral simulations is the number of variables that can be estimated in the course of the minimization procedure. Column 5 in Table 3 presents the number of parameters that were varied in our simulations. This number includes (i) the parameters of rotational mobility, (ii) the values describing the Gaussian and Lorentzian line widths, (iii) the parameters of the local potential, (iv) the tilt angles of the main rotation axis in the molecular magnetic frame when it was necessary, (v) the quasi-libration amplitudes (if used), and (vi) values describing the macroscopic orientation distribution. Thus, the shown numbers of variables are relatively large. Hence, the important questions are how many parameters can be estimated in the course of simulation and whether it is possible to estimate this set of parameters with desirable reliability. Answers to these questions are obtained by analysis of the covariation matrix for all parameters. This matrix provides estimations of the errors for the obtained values and the interdependence of the variables. On the basis of the obtained covariation matrixes for the presented simulations, we have come to following conclusions:

(i) In all cases presented, the set of simulated spectra permits estimation of the chosen number of parameters. The minimization procedure was checked to converge to the stable minimum, optimal with respect to all varied parameters.

(ii) There is often a strong interdependence between the rotational diffusion coefficients and the line width parameters. This obvious dependence should be overcome by using zero Lorentzian broadening, especially if the rotation characteristics are the values of interest. The noticeable correlation can be seen often between rotational diffusion coefficients and other characteristics of rotation, namely, angles describing the direction of the principal rotation axis and amplitudes of librations. This circumstance makes the estimation of rotational characteristics not very reliable.

(iii) Characteristics of orientational alignment (order parameters) ordinarily do not demonstrate a noticeable correlation with characteristics of rotational mobility; they are determined more reliably.

(iv) The uncertainty ranges obtained from the covariation matrixes are considerably smaller than the real errors of determination. The most reliable estimation of uncertainty is achieved by a special set of simulations performed with shifting of the tested parameter from the optimal value. The procedure for such estimation of errors is described in detail in ESI.V. The different variable parameters were found to be determined with different uncertainties. For example, characteristics of the global orientation distribution are determined with relatively high accuracy, while the local potential is estimated very roughly (see the correlation coefficients in Table S3). Typical errors of different values are presented above in section II.

The used method is based on the estimation of a very large number of parameters by simulation of the experimental spectra. As can be seen in Table 3, this number may be as high as 60−70 parameters. Evidently, the number of determined parameters should be justified by the amount of independent experimental data. Quantitative estimation of this amount cannot be done in a general form and requires special consideration in each particular case. However, a rough estimation in the case of EPR spectroscopy can be the following. When a one-component EPR spectrum is considered, at least three values are observable and measurable from the spectrum: the amplitude, width, and position of the component. The EPR signal of nitroxide radical is a three-component spectrum because of the hyperfine structure. Thus, up to nine values are easily measurable for one spectrum. In the case of the considered angular dependences for liquid crystals (e.g., shown in Figure 4), 10−20 spectra at distinct sample orientations are substantially different and therefore

DOI: 10.1021/acs.jpcb.9b05431
J. Phys. Chem. B 2019, 123, 5875−5891

Table 4. Examples of Magnetic Parameters Averaged by Fast Quasi-Libration Motion in Accordance with Equation 7 (Hyperfine Coupling Parameters Are in Gauss)

			initial			averaged		
system	probe/LC	librations $L_x/L_y/L_z$ (deg)	g_{xx}, A_{xx}	g_{yy}, A_{yy}	g_{zz}, A_{zz}	g_{xx}, A_{xx}	g_{yy}, A_{yy}	g_{zz}, A_{zz}
6	A3/HOPDOB 353 K (SmA)	0.0/23.9/0.0	2.0093, 4.1	2.0065, 5.7	2.0018, 32.98	2.00888, 5.71	2.0065, 5.70	2.00222, 31.37
7	A4/HOPDOB 353 K (SmA)	1.8/0/60.8	2.0091, 3.5	2.0066, 5.9	2.0026, 33.34	2.00835, 4.21	2.0065, 5.19	2.00222, 31.33
8	A5/HOPOOB, 355 K (N)	44.3/0/66.7	2.0097, 7.0	2.0068, 4.8	2.0023, 34.17	2.00870, 6.24	2.00700, 10.75	2.00310, 28.97
9	A5/HOPDOB, 353 K (SmA)	32.4/0/73.2	2.0097, 5.9	2.0068, 5.8	2.0023, 34.17	2.00856, 5.86	2.00749, 8.68	2.00275, 31.33
10	A5/H59 347 K (SmA)	50.5/0/68.1	2.0097, 5.9	2.0068, 5.8	2.0023, 34.17	2.00867, 5.86	2.00683, 12.13	2.00329, 27.87
11	A5/H59 340 K (SmB)	56.9/0/64.3	2.0097, 5.9	2.0068, 5.8	2.0023, 34.17	2.00876, 5.87	2.00653, 13.47	2.00351, 26.53
12	A5/8CB 308 K (N)	0/0/70.1	2.0097, 6.95	2.0068, 4.91	2.0023, 34.17	2.00863, 6.19	2.00787, 5.66	2.00230, 34.17

Table 5. Rotational Diffusion Tensors Estimated by Simulation of EPR Spectra

probe/LC	model	$D_x = D_y$	D_z	β_D (deg)[a]	γ_D (deg)[a]
I. Large Elongated Probes in Aligned Liquid Crystals					
CSL/5CB, 305 K (N)	MF	$(2.1 \pm 0.2) \times 10^7$	$(3.9 \pm 0.4) \times 10^8$	90	113.6 ± 0.9
	ODF	$(5.1 \pm 1.9) \times 10^7$	$(3.1 \pm 0.7) \times 10^8$	90	114.0 ± 1.6
C4/8CB, 299 K (SmA)	MF	$(0.5–3.0) \times 10^6$	$(4.2 \pm 0.5) \times 10^8$	39.9 ± 1.4	90
	ODF	$(3.9 \pm 1.4) \times 10^6$	$(5.0 \pm 0.6) \times 10^8$	38.6 ± 1.0	90
C11/8CB, 300 K (SmA)	MF	1.6×10^6	3.5×10^8	37	90
	ODF	$(0.9–2.7) \times 10^6$	$(4.1 \pm 0.5) \times 10^8$	38.1 ± 1.0	90
II. Small Probes in Aligned Liquid Crystals					
A3/HOPDOB 353 K (SmA)	ODF	$(3.2 \pm 1.6) \times 10^8$	$(0.7–2.5) \times 10^9$	99.7 ± 2.6	-44.0 ± 2.9
A4/HOPDOB 353(SmA)	ODF	$(4.6 \pm 1.3) \times 10^8$	$(6.8 \pm 0.5) \times 10^8$	92.7 ± 3.4	85.7 ± 4.1
A5/HOPOOB, 355 K (N)	ODF	$(0.8–3.3) \times 10^9$ [b]		90	90
A5/HOPDOB, 353 K (SmA)	ODF	$(2.2 \pm 0.5) \times 10^9$ [b]		90	90
A5/H59 347 K (SmA)	ODF	$(2.1 \pm 0.7) \times 10^9$ [b]		90	90
A5/H59 340 K (SmB)	ODF	$(3.8 \pm 0.4) \times 10^9$ [b]		90	90
A5/8CB 308 K (N)	ODF	$(4.6 \pm 1.2) \times 10^8$ [b]		90	90

[a]The Euler angles $(0, \beta_D, \gamma_D)$ connect the **g** tensor molecular frame with the orientation molecular frame coinciding with the rotation molecular frame. Some values of the angles β_D and γ_D that were found to be equal to 90° were not varied. [b]Anisotropy of rotation does not matter within the errors of determination.

form a set of independent data. As a result, it is possible to expect that the angular dependence gives enough information for the determination of a set of more than 100 parameters. Taking into account more complex line shapes and the possible appearance of additional spectral lines, one can conclude that the above estimation gives a lower bound for the possible number of determined parameters. The results of this consideration are in accordance with our practice of simulation of experimental EPR spectra.

IV.2. Characteristics of Rotational Mobility of Probe Molecules in Liquid Crystals. Characteristics of rotational mobility of radicals in different media are commonly obtained by analysis of EPR spectra of unordered samples. In the case of an aligned sample of a liquid crystal, recording spectra for different sample orientations relative to the magnetic field produces more information. Therefore, the simulations of the angular dependence produce a more reliable description of molecular mobility and allow the possibilities and limitations of the methods used to be ascertained.

Table 3 demonstrates that in the case of spin probes with molecular sizes larger than the size of the liquid crystal molecules, the rotational diffusion mechanism satisfactorily describes the experimental EPR spectra. As shown above, in the cases of smaller probes or higher temperatures, the more complicated molecular rotation mechanism including rotational jumps is necessary. One can expect that rotational jumps are a common property of molecules in liquid crystals because liquid crystals are structured media. Brownian rotational diffusion is an appropriate approximation only for cases of jumps with low frequency on the EPR time scale or jumps with small amplitudes. In other cases, the rotational jumps of the probe molecules within the cages of the liquid-crystalline medium should be considered explicitly. System 5 (Table 3) is an example of a case where the rotational jumps should be considered even for a probe with a large size. Unfortunately, calculation of the spectra using the stochastic Liouville equation in the cases of rotational jumps in the anisotropic medium is not feasible, as it requires a huge set of orthogonal functions and has tremendous computational cost. Generally, the SRLS model suggested earlier[72,73] should be used in these cases. This approach combines the relatively fast intracage rotation moves and the slower diffusive reorganization of the surroundings of the probe. To diminish the computational effort to a reasonable level, in present work we used a simplified model in which the frequency of intracage rotational moves is assumed to be sufficiently high to average the parameters of the spin Hamiltonian. In this case the intracage rotational jumps can be described as effective quasi-libration

DOI: 10.1021/acs.jpcb.9b05431
J. Phys. Chem. B 2019, 123, 5875−5891

moves. Thus, the rotational molecular mobility was divided into two parts: intracage quasi-librations describing mainly the properties of the probe molecule and the diffusion tensor characterizing the liquid-crystalline medium. The expressions in eq 7 for the averaged magnetic parameters are based on results from refs 20 and 74 (presented in section II). It is possible to consider libration moves around three molecular axes. The simulations of EPR spectra have shown that librations around one or two molecular axes are ordinarily enough to describe the experimental spectra. Typical quasi-libration amplitudes are collected in Table 4. It can be seen that the values of the amplitudes estimated by spectral simulations ordinarily lie in the range 50−70°. This means that the local symmetry of the liquid-crystalline medium is often approximately hexagonal and that the intracage rotation of small molecules corresponds to jumps by ∼60° between two almost equivalent positions in the local structure.

In accordance with assumption used for the derivation of eq 7, the nitroxide radicals are distributed uniformly within the angular range limited by the quasi-libration amplitude. Examples of the magnetic parameters averaged over this distribution are presented in Table 4. The table demonstrates relatively small changes in the magnetic parameters induced by fast intracage quasi-librations.

The slower diffusive relaxation of the liquid-crystalline cage was described by the rotational diffusion tensor. The obtained components of the tensor and the angles describing the main molecular rotation axis (β_D and γ_D) are listed in Table 5. In the cases of elongated probe molecules, both the perpendicular ($D_{perp} = D_x = D_y$) and parallel ($D_{par} = D_z$) components of the rotational diffusion tensor were determined. The obtained value of D_{perp} demonstrates a reasonable dependence on the length of the probe molecule. The determined direction of the principal rotation axis is close to the long molecular axis of the radical. Independent determination of D_x and D_y is rarely possible.

IV.3. Orientation Distributions of Probes in Liquid Crystals. The orientation distribution of molecules in the sample frame is described by eqs 3 and 6 containing the set of order parameters P_{jmn}. In the case of the MF model, only order parameters with zero index m are nonzero, as an axial distribution of probes relative to the director of the liquid crystal is assumed. The MF model describes the orientation distribution by eq 1 containing the coefficients of the potential, c_{jn}. The case where the only nonzero coefficients are c_{j0} (most often c_{20}) corresponds to axial molecules. As the sample in the MF approach is axial, only the order parameters P_{j00} are nonzero. The nonzero coefficient c_{22} (and other coefficients with nonzero index n) describe biaxial ordering of probes in the local potential. This corresponds to the dependence of the orientation distribution on the angle γ_l. Such cases will be named below as "molecular biaxiality".

In the case of the ODF model, the additional distribution of the local director in the sample frame is taken into account. Different sets of order parameters are necessary for description of samples with different ODF symmetry. The order parameters with zero index m are nonzero in the case of axial samples. Orthorhombic samples require order parameters with even index m. Additional parameters with odd index m are necessary for description of non-orthorhombic samples. As a result, the number of variables for spectral simulation strongly depends on the symmetry of the sample. This dependence is reflected in Table 3 by the large numbers of variables for systems 7, 8, and 15−17.

The local molecular orientation distribution and the orientation distribution of the director in the sample can be analyzed separately. The values of the coefficients describing the potential of the medium at the point of localization of the probe molecule are collected in Table 6.

Table 6. Values of Potentials Used for Simulation of EPR Spectra

system	probe/LC	model	c_{20}	c_{22}
	Well-Aligned Probes			
1	CSL/5CB, 305 K (N)	MF	2.8 ± 0.4	0.4−1.3
		ODF	3.6 ± 1.9	0.2−3.0
2	C4/8CB, 299 K (SmA)	MF	7.2 ± 0.8	2.5 ± 0.4
		ODF	15.1 ± 9.4	9.1 ± 8.7
3	C11/8CB, 300 K (SmA)	MF	5.3 ± 0.7	1.2 ± 0.3
		ODF	13.2 ± 2.5	6.8 ± 1.9
4	CSL/HOPDOB, 354 K (SmA)	MF	4.4 ± 1.1	0.6 ± 0.4
		ODF	4.4 ± 1.5	0.1−0.6
	Small Probes in Well-Aligned Liquid Crystals			
6	A3/HOPDOB 353 K (SmA)	ODF	9.0	8.2
7	A4/HOPDOB 353 K (SmA)	ODF	8.1 ± 1.9	3.5−7.0
8	A5/HOPDOB, 353 K (SmA)	ODF	12.8 ± 1.6	12.4 ± 3.4
9	A5/HOPOOB, 355 K (N)	ODF	3.1 ± 2.5	0
10	A5/H59 347 K (SmA)	ODF	23.4 ± 1.8	0
11	A5/H59 340 K (SmB)	ODF	15.0 ± 1.0	0−3.0
12	A5/8CB 308 K (N)	ODF	6.5 ± 1.3	5.6 ± 1.3
	Dual Localization of the Probe in the LC Structure			
13	A5/8CB, 303 K (SmA)	ODF	c_{20} = 1.0	c_{22} = −0.3
			c_{40} = 1.6	c_{42} = 1.2
				c_{44} = 0.4
14	A1/8CB, 301 K (SmA)	ODF	c_{20} = 0.8	c_{22} = 1.4
			c_{40} = 2.3	c_{42} = 1.7
15	C4/HOPDOB, 354 K (SmA)	ODF	$c_{20}(1)$ = 4.9	$c_{22}(1)$ = 1.2
			$c_{20}(2)$ = 3.3	$c_{22}(2)$ = 0.0

The simulation of EPR spectra was found to have low sensitivity to the local potential. In the case of the most mobile probe, A5, in high-temperature liquid crystals, the spectra are almost independent of c_{20} in the range c_{20} = 5−20. In the cases of smaller rotational mobility, the discrepancy demonstrates the gentle minimum that permits estimation of the c_{20} and c_{22} values presented in the Table 6. The reliability of the obtained values remains poor because the simultaneous changing of c_{20} and c_{22} feebly influences the spectra. A strong interdependence of the c_{20} and c_{22} coefficients is often observed (Table S3). This correlation impedes the determination of errors for these coefficients and makes the uncertainties the Table 6 unreliable. When three or more potential terms c_{jn} are used, the mutual intercorrelations make the estimation of the uncertainties impossible and useless. Nevertheless, our simulations yield the following conclusions:

(i) The value of c_{20} is not restricted to the range of 1−5 often used.

(ii) Satisfactory simulation of spectra often becomes impossible with c_{22} = zero. This corroborates the existence of molecular biaxiality of the probes in the liquid-crystalline medium.

DOI: 10.1021/acs.jpcb.9b05431
J. Phys. Chem. B 2019, 123, 5875−5891

(iii) The values of the potential seem to be lower for nematic mesophases than for smectic ones.

A typical local orientation distribution is presented in Figure 6a,b. The functions in Figure 6 present distributions of the local director in the molecular coordinate frame in accordance with eq 1. This is the only method for three-dimensional (3D) visualization of molecular biaxiality. This biaxiality is seen in Figure 6b as oblateness of the projection in the *xy* plane.

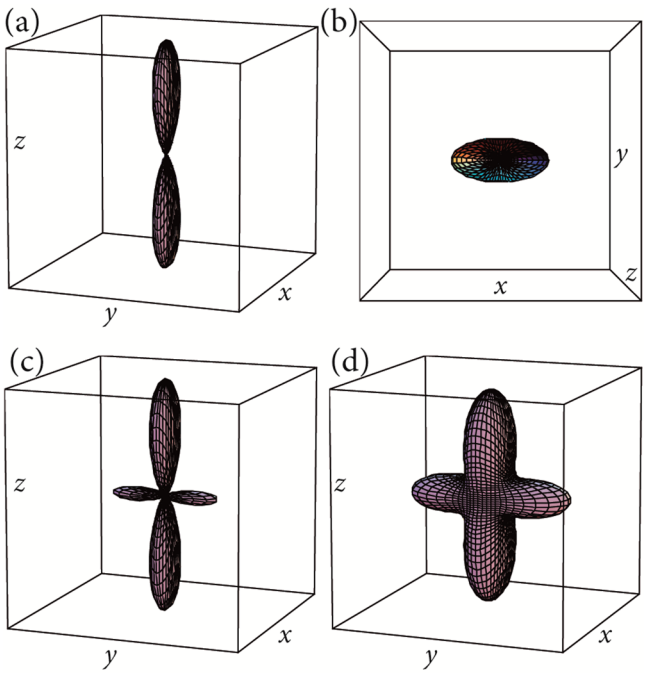

Figure 6. Orientation distributions of the local director in the molecular coordinate frame: (a, b) typical local orientation distribution (A4/HOPDOB, system 7) in different projections; (c) dual orientation of probe A5 in 8CB; (d) same as (c) presented as $\rho(\alpha,\beta,\gamma)^{1/3}$.

The two possible orientations of probe A5 in the liquid crystal are shown in Figure 6c as the orthogonal lobes. To estimate visually the relative population of these two orientations, the distribution function is presented as $\rho(\alpha,\beta,\gamma)^{1/3}$ in Figure 6d. The ratio of volumes for different lobes in this picture demonstrates the populations of different probe orientations. The complicated local orientation distribution shown in Figure 6c,d is described by nonzero higher-rank coefficients c_{40}–c_{44} in eq 1. In general, the use of these coefficients very rarely leads to better simulations of EPR spectra. This situation is apparently realized when the transition from one possible orientation to another proceeds with relatively low frequency but cannot be approximated as rotational diffusion.

If the frequency of the transitions is negligible, the different probe orientations can be seen in the shape of global orientation distribution of the probe in the sample. This situation was observed in the case of A1/8CB (system 14). A more general approach for simulations of spectra in this case is the explicit simulation of the spectra as sums of spectra for two independent orientations. This approach was successfully applied for simulation of spectra C4/HOPDOB (system 15). The spectra for the system and the results of the simulation are presented in Figure S8. For this system it was found that the different orientations of the probe differ additionally by the values of the potential and the parameters of rotational mobility. Obviously, the two states of the probe correspond to different positions in the spatially inhomogeneous SmA structure. This result is in accordance with the previously published conclusion.[95]

Examples of obtained parameters of the global orientation distribution are presented in Table 7. The table demonstrates that the ODF and MF models equally describe the orientation distributions in systems 1, 2, and 4. The MF simulation of the spectra for probe A5 was marked in Table 3 as producing "baseless" parameters of rotational mobility. In Table 7 one can see that these simulations nevertheless give characteristics of the orientation distribution quite similar to the values obtained using the ODF model. The simulation of system 6 using MF was marked in Table 3 as "failed" because the calculated spectra deviated from the experimental ones. The orientation distribution in this case noticeably differs from the distribution obtained using the more successful ODF simulation.

In Table S4 one can find the temperature dependence of the orientation distribution for the CSL/5CB in the nematic phase (system 1). Both the rotational and orientational characteristics in the table demonstrate physically reasonable temperature dependences. The values using by MF and ODF methods for this system are close and show similar temperature dependences.

The molecular biaxial order parameters P_{j0n} are not shown in Table 7. When these values are determined from EPR spectra, they are in the range 0.002–0.10, as exemplified in ESI.VIII. They diminish for larger values of index *j*. These values obtained using the MF and ODF models are similar for the systems marked in Table 3 as "satisfactory", but they become irreproducible in the cases marked as "failed" or "baseless" (see Table S6).

Table 7. Local Orientation Distributions of the Principal Molecular Rotation Axis (Principal Molecular Orientation Axis)

	CSL/5CB, 305 K (N) system 1		C4/8CB,299K(SmA) system 2		CSL/HOP-DOB 354 K (SmA) system 4		A5/H59, 347 K (SmA) system 10		A5/8CB, 308 K (N) system 12		A3/HOP-DOB, 353 K (SmA) system 6	
	ODF	MF	ODF	MF	ODF	MF	ODF	MF	ODF	MF	ODF	MF
$P_{2,0,0}$	0.522	0.511	0.812	0.837	0.698	0.736	0.585	0.530	0.575	0.589	0.577	0.696
$P_{4,0,0}$	0.154	0.132	0.556	0.567	0.347	0.396	0.218	0.186	0.240	0.233	0.248	0.400
$P_{6,0,0}$	0.028	0.011	0.328	0.321	0.131	0.165	0.056	0.048	0.085	0.069	0.098	0.215
$P_{8,0,0}$	0.004	−0.003	0.164	0.156	0.040	0.056	0.015	0.010	0.027	0.016	0.039	0.114
$P_{10,0,0}$	–	–	0.069	0.067	0.010	0.016	0.004	0.002	0.008	0.003	0.015	0.060
$P_{12,0,0}$	–	–	0.026	0.026	0.002	0.004	–	–	0.002	–	0.006	0.030
$P_{14,0,0}$	–	–	0.007	0.009	–	–	–	–	–	–	0.002	0.015

DOI: 10.1021/acs.jpcb.9b05431
J. Phys. Chem. B 2019, 123, 5875–5891

Table 8. Orientation Distribution of the Local Director in the Axial Liquid Crystals

	CSL/5CB (N) system 1	C4/8CB (SmA) system 2	A5/8CB (SmA) system 13	A5/8CB (N) system 12	CSL/HOPDOB (SmA) system 4	A5/H59 (SmA) system 10	C4/HOPDOB (SmA) system 15
$Psam_{2,0,0}$	0.79	0.90	0.86	0.89	0.94	0.61	0.76
$Psam_{4,0,0}$	0.50	0.76	0.82	0.72	0.87	0.25	0.47
$Psam_{6,0,0}$	0.25	0.62	0.71	0.53	0.79	0.08	0.31
$Psam_{8,0,0}$	0.11	0.46	0.63	0.36	0.71	0.03	024
$Psam_{10,0,0}$	0.04	0.31	0.52	0.24	0.63	0.01	0.18
$Psam_{12,0,0}$	0.01	0.19	0.43	0.15	0.53	–	0.13
$Psam_{14,0,0}$	−0.003	0.10	0.33	0.10	0.43	–	0.09
$Psam_{16,0,0}$	–	0.03	0.26	0.06	0.34		0.06
$Psam_{18,0,0}$	–	–-	0.17	0.03	0.25		0.02

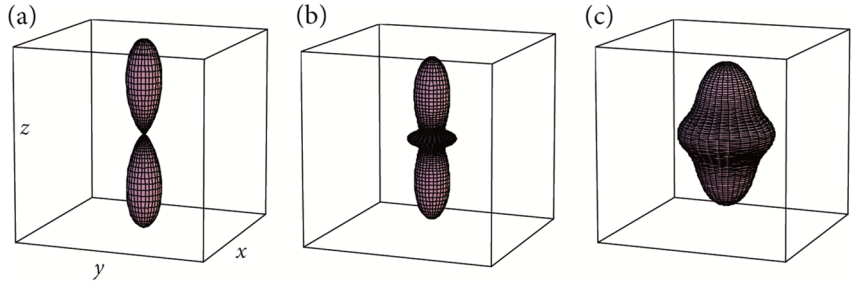

Figure 7. Axial orientation distributions of the molecular main axis in the sample frame: (a) CSL/5CB 297 K (N); (b) A1/8CB; (c) same as (b) presented as $\rho(\alpha,\beta,\gamma)^{1/3}$.

The ODF method allows separate determination of the local orientation distribution and the orientation distribution of the local director in the sample. The order parameters for the latter are presented in Table 8. Table 8 demonstrates the relatively high ordering in the liquid-crystalline samples, although the director is not perfectly aligned as was assumed earlier.[15] The order parameters in Table 8 characterize the quality and homogeneity of the samples. Imperfection of these distributions obviously is the result of both defects in sample preparation and thermodynamic fluctuations of the local director in the liquid crystal.

Tables 7 and 8 present the ranks of the order parameters that are meaningful in the description of the orientation distribution. In the cases of relatively poor orientational alignment, the order parameters up to rank j = 8−10 are sufficient. For ordered liquid crystals, it was found that mostly the order parameters up to rank 12−14 are essential. When well-aligned materials are described, order parameters up to j = 18 or even higher become meaningful and therefore can be determined from experimental EPR spectra.

The characteristics presented in Table 7 are full descriptions of the orientation distributions in the case of axial molecules in the axial liquid crystal. On the basis of the presented data, one can conclude that the model-free ODF method confirms the mean-field potential approach only for description of the uniformly aligned axial liquid crystals at low temperature with large-sized probe molecules.

On the other hand, more interesting is the problem of describing more complicated distributions. In the cases of macroscopically biaxial samples (orthorhombic sample symmetry), the order parameters with nonzero even index m became substantial. In the cases of sample symmetry lower than orthorhombic, additional parameters with odd index m should be considered. The distributions in these cases are characterized by a large number of order parameters with different indices j and m (see ESI.IX). Therefore, a more adequate method of presenting such a distribution is 3D visualization. In Figure 7 the orientation distributions of the principal molecular orientation axis in the sample coordinate frame are presented. The typical distribution for an axial sample is shown in Figure 7a for comparison. The distribution demonstrating the dual orientation of probe A1 in the liquid crystal 8CB is shown in Figure 7b. The presentation as $\rho(\alpha,\beta,\gamma)^{1/3}$ in Figure 7c visually shows the populations of different orientations as relative volumes of different lobes in this picture.

A sample with orthorhombic symmetry was observed in the present work in the case of A5/HOPDOB (SmA). This system was found to be sensitive to the temperature gradient occurring in course of cooling of the sample from the oriented nematic to the smectic phase. For the thin-layer sample, the orthorhombic distortion was almost invisible in the resulting distribution. On the contrary, for the bulk sample in a 4 mm-diameter ampule, the sample acquired clear orthorhombic symmetry. This feature manifested itself in the appearance of additional small components in the EPR spectra. Nevertheless, spectra recorded upon turning the sample to any angle clockwise or counterclockwise relative to the sample axis were the same, proving the orthorhombic properties. The orientation distribution obtained by simulation of the spectra is shown in Figure 8. This distribution shape is described by sample biaxial order parameters presented in ESI.IX.

The sample with symmetry lower than orthorhombic was prepared by the following procedure. The homeotropic nematic layer sample (thickness 25 μm) was exposed to a magnetic field directed perpendicular to the director of the liquid crystal. After that the sample was cooled to the smectic phase. The obtained sample demonstrates strong angular dependence of the EPR spectrum, as illustrated in Figure 9. The analysis of this angular dependence shows that there are no orthorhombic axes in this sample. This can be illustrated by comparison of the spectra for 30° and 150° (Figure 9). For

DOI: 10.1021/acs.jpcb.9b05431
J. Phys. Chem. B 2019, 123, 5875−5891

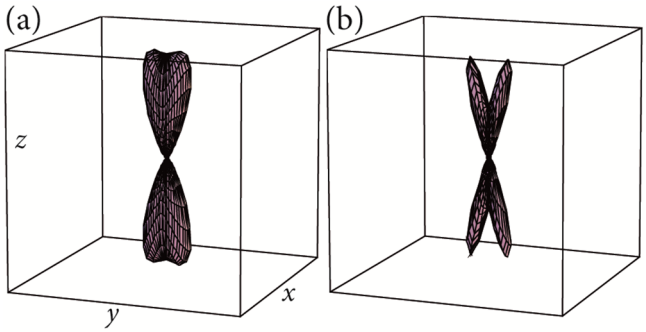

Figure 8. Orthogonal orientation distribution for A5/HOPDOP in the bulk SmA (system 16): (a) global distribution of the molecular axis in the sample frame; (b) distribution of the local director in the sample frame.

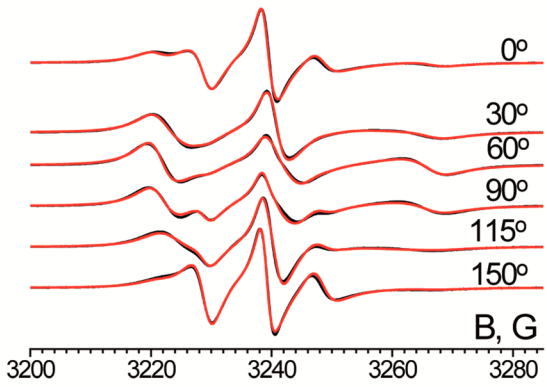

Figure 9. Angular dependence of the experimental EPR spectra of C4/8CB 297 K (SmA) for a non-orthorhombic sample prepared at 12 000 G (black lines) and results of the simulations (red lines).

orthorhombic symmetry, the spectra should be identical for any pair of orientations (α, 180°−α). This symmetry is not observed for the spectra in Figure 9.

The orientation distributions extracted by simulations of EPR spectra depend on the magnetic field strength used in the course of preparing the sample. Figure 10 illustrates this dependence. It can be seen that a part of the liquid-crystalline sample keeps the initial orientation caused by the anchoring surface. However, another part forms the smectic structure with a turned director that does not coincide with either of the competing orienting actions, namely, the anchoring surface and the magnetic field. This example demonstrates that the suggested method is suitable for investigation of samples with arbitrary symmetry.

V. CONCLUSION

Independent consideration of the local orientational potential and the distribution of the local directions in the sample transforms a procedure of quantitative simulation of EPR spectra into a model-free method. This method allows more reliable data to be obtained concerning molecular orientational order and molecular rotational mobility. The quantitative simulation of spectra demonstrate that the ordinarily used model of rotational diffusion in a mean-field potential is appropriate for describing molecular mobility and orientational ordering only for well-ordered, low-mobility, highly viscous liquid crystals at relatively low temperatures with spin probes

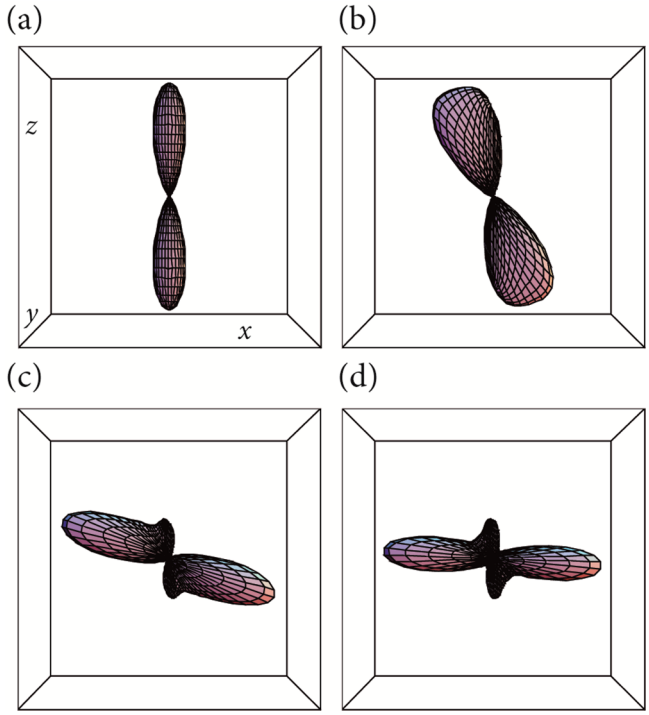

Figure 10. Orientation distributions in the case of C4/8CB non-orthorhombic liquid crystal after cooling of the layer from the homeotropic nematic phase to the smectic A phase under perpendicular magnetic fields of (a) 0 G, (b) 9000 G, (c) 12 000 G, and (d) 14 700 G.

of large size. In cases of higher molecular mobility, the angular jump mechanism of molecular moves should be considered. This mechanism was found to be approximately described as quasi-librations in cases of high frequency of molecular jumps. Thus, explicit consideration of the difference between the microscopic local molecular orientation and the global orientational alignment of the sample as well as the difference between high-frequency molecular moves and slower reorganization of the medium is necessary to obtain a quantitative description of the experimental data and reliable characteristics.

The orientation distribution function was found to be experimentally characterized by a set of order parameters up to 18th rank. Orientation distributions with arbitrary symmetry can be examined in detail using the suggested approach with quantitative determination of biaxial parameters.

■ ASSOCIATED CONTENT

Supporting Information

The Supporting Information is available free of charge on the ACS Publications website at DOI: 10.1021/acs.jpcb.9b05431.

ESI.I. Formulas for global orientational order parameters; **ESI.II.** Determination of the magnetic parameters of radicals in liquid-crystalline media by means of simulation of unordered samples in the rigid limit; **ESI.III.** Determination of the maximum rank of the orientation distribution function; **ESI.IV.** Derivation of eq 7; **ESI.V.** General technique used for estimation of uncertainties of parameters; **ESI.VI.** Experimental spectra and results of simulation for system 15 (C4/HOPDOB 354 K (SmA)); **ESI.VII.** Temperature dependence of the orientation distribution for CSL/

DOI: 10.1021/acs.jpcb.9b05431
J. Phys. Chem. B 2019, 123, 5875−5891

5CB in the nematic phase (system 1); **ESI.VIII.** Local molecular biaxiality parameters; **ESI.IX.** Order parameters for samples with biaxial distortions (orthorhombic and non-orthorhombic samples) (PDF)

AUTHOR INFORMATION

Corresponding Author

*E-mail: a.kh.vorobiev@gmail.com.

ORCID

A. Kh. Vorobiev: 0000-0002-6701-0524

A. V. Bogdanov: 0000-0003-1044-4783

Notes

The authors declare no competing financial interest.

The software developed by the authors to simulate EPR spectra of spin probes in ordered samples can be downloaded from the website https://sourceforge.net/projects/odfr/.

ACKNOWLEDGMENTS

The authors are grateful to Prof. R. Tamura (Kyoto University) and Prof. S. Bottle (Queensland University of Technology) for provision of the spin probes. This work was supported by the Russian Foundation for Basic Research (Grants 18-29-19120 mk, 16-33-60139 mol_a_dk, and 19-02-00765) and in part by the M. V. Lomonosov Moscow State University Program of Development.

REFERENCES

(1) Bhat, S. N.; Sharma, A.; Bhat, S. V. Vitrification and Glass Transition of Water: Insights from Spin Probe ESR. *Phys. Rev. Lett.* **2005**, *95*, 235702−1−235702−4.

(2) Zager, S. A.; Freed, J. H. Electron Spin Relaxation and Molecular Dynamics in Liquids. II. Density Dependence. *J. Chem. Phys.* **1982**, *77*, 3360−3375.

(3) Stoesser, R.; Herrmann, W.; Zehl, A.; Strehmel, V.; Laschewsky, A. EPR Spin Probes in Ionic Liquids. *ChemPhysChem* **2006**, *7*, 1106−1111.

(4) Robinson, B. H.; Haas, D. A.; Mailer, C. Molecular Dynamics in Liquids: Spin-Lattice Relaxation of Nitroxide Spin Labels. *Science* **1994**, *263*, 490−493.

(5) Paschenko, S. V.; Toropov, Yu. V.; Dzuba, S. A.; Tsvetkov, Yu. D.; Vorobiev, A. Kh. Temperature Dependence of Amplitudes of Libration Motion of Guest Spin-Probe Molecules in Organic Glasses. *J. Chem. Phys.* **1999**, *110*, 8150−8154.

(6) Spielberg, J. I.; Gelerinter, E. Further Studies on the Molecular Dynamics of the Glass Transition and the Glass State Using EPR Probes. *Phys. Rev. B: Condens. Matter Mater. Phys.* **1984**, *30*, 2319−2333.

(7) Dzuba, S. A.; Tsvetkov, Y. D.; Maryasov, A. G. Echo-Induced EPR Spectra of Nitroxides in Organic Glasses: Model of Orientational Molecular Motions Near Equilibrium Position. *Chem. Phys. Lett.* **1992**, *188*, 217−222.

(8) Alessi, L.; Andreozzi, L.; Faetti, M.; Leporini, D. Anisotropic Jump Model of the Rotational Dynamics in Glasses. *J. Chem. Phys.* **2001**, *114*, 3631−3639.

(9) Kovarski, A. L. *Molecular Dynamics of Additives in Polymers*; VSP: Utrecht, The Netherlands, 1997.

(10) Yampolskii, Y. P.; Motyakin, M. V.; Wasserman, A. M.; Masuda, T.; Teraguchi, M.; Khotimskii, S.; Freeman, B. D. Study of High Permeability Polymers by means of the Spin Probe Technique. *Polymer* **1999**, *40*, 1745−1752.

(11) Chernova, D. A.; Vorobiev, A. Kh. Molecular Mobility of Nitroxide Spin Probes in Glassy Polymers. Quasi-libration model. *J. Polym. Sci., Part B: Polym. Phys.* **2009**, *47*, 107−120.

(12) *Advanced ESR Methods in Polymer Research*; Wiley-Interscience: Hoboken, NJ, 2006.

(13) Miller, W. G. Spin-Labeled Synthetic Polymers. In *Spin Labeling: Theory and Applications*; Berliner, L. J., Ed.; Academic Press: New York, 1976; pp 173−221.

(14) Chernova, D. A.; Vorobiev, A. K. Molecular Mobility of Nitroxide Spin Probes in Glassy Polymers: Models of the Complex Motion of Spin Probes. *J. Appl. Polym. Sci.* **2011**, *121*, 102−110.

(15) Wassmer, K.-H.; Ohmes, E.; Portugall, M.; Ringsdorf, H.; Kothe, G. Molecular Order and Dynamics of Liquid-Crystal Side-Chain Polymers: an Electron Spin Resonance Study Employing Rigid Nitroxide Spin Probes. *J. Am. Chem. Soc.* **1985**, *107*, 1511−1519.

(16) Maresch, G. G.; Weber, M.; Dubinskii, A. A.; Spiess, H. W. 2D-ELDOR Detection of Magnetization Transfer of Nitroxides in Disordered Solid Polymers. *Chem. Phys. Lett.* **1992**, *193*, 134−140.

(17) Borbat, P. P.; Costa-Filho, A. J.; Earle, K. A.; Moscicki, J. K.; Freed, J. H. Electron Spin Resonance in Studies of Membranes and Proteins. *Science* **2001**, *291*, 266−269.

(18) Isaev, N. P.; Syryamina, V. N.; Dzuba, S. A. Small-Angle Orientational Motions of Spin-Labeled Lipids in Cholesterol-Containing Bilayers Studied at Low Temperatures by Electron Spin Echo Spectroscopy. *J. Phys. Chem. B* **2010**, *114*, 9510−9515.

(19) McConnel, H. M. Molecular Motion in Biological Membranes. In *Spin Labeling: Theory and Applications*; Berliner, L. J., Ed.; Academic Press: New York, 1976; pp 525−560.

(20) Griffith, O. H.; Jost, P. C. Lipid Spin Labels in Biological Membranes. In *Spin Labeling: Theory and Applications*; Berliner, L. J., Ed.; Academic Press: New York, 1976; pp 453−521.

(21) Longhi, S.; Belle, V.; Fournel, A.; Guigliarelli, B.; Carriere, F. Probing Structural Transitions in Both Structured and Disordered Proteins Using Site-Directed Spin-Labeling EPR Spectroscopy. *J. Pept. Sci.* **2011**, *17*, 315−328.

(22) Barnes, J. P.; Liang, Z.; Mchaourab, H. S.; Freed, J. H.; Hubbell, A. L. A Multifrequency Electron Spin Resonance Study of T4 Lysozyme Dynamics. *Biophys. J.* **1999**, *76*, 3298−3306.

(23) Robinson, B.; Thomann, H.; Beth, A.; Fajer, P.; Dalton, L. Applications of EPR and Advanced EPR Techniques To Study of Protein Structure and Interactions. In *EPR and Advanced EPR Studies of Biological Systems*; Dalton, L., Ed., CRC Press: Boca Raton, FL, 1985; pp 183−256.

(24) Schiemann, O.; Cekan, P.; Margraf, D.; Prisner, T. F.; Sigurdsson, S. Th. Relative Orientation of Rigid Nitroxides by PELDOR: Beyond Distance Measurements in Nucleic Acids. *Angew. Chem., Int. Ed.* **2009**, *48*, 3292−3295.

(25) Fielding, A. J.; Concilio, M. G.; Heaven, G.; Hollas, M. A. New Developments in Spin Labels for Pulsed Dipolar EPR. *Molecules* **2014**, *19*, 16998−17025.

(26) Krumkacheva, O.; Bagryanskaya, E. EPR-Based Distance Measurements at Ambient Temperature. *J. Magn. Reson.* **2017**, *280*, 117−126.

(27) Bartucci, R.; Erilov, D. A.; Guzzi, R.; Sportelli, L.; Dzuba, S. A.; Marsh, D. Time-Resolved Electron Spin Resonance Studies of Spin-Labeled Lipids in Membranes. *Chem. Phys. Lipids* **2006**, *141*, 142−157.

(28) Jeschke, G. DEER Distance Measurements on Proteins. *Annu. Rev. Phys. Chem.* **2012**, *63*, 419−446.

(29) Seelig, J. Spin Label Studies of Oriented Smectic Liquid Crystals (A Model System for Bilayer Membranes). *J. Am. Chem. Soc.* **1970**, *92*, 3881−3887.

(30) Luckhurst, G. R.; Setaka, M.; Zannoni, C. An Electron Resonance Investigation of Molecular Motion in the Smectic A Mesophase of a Liquid Crystal. *Mol. Phys.* **1974**, *28*, 49−68.

(31) Bikchantaev, I. G.; Konstantinov, V. N.; Ovchinnikov, I. V. Angular Dependence of the ESR Spectra of Copper Complexes in an Oriented Vitreous Liquid Crystal. *J. Struct. Chem.* **1977**, *17*, 705−709.

(32) Fryburg, G. C.; Gelerinter, E. Electron Paramagnetic Resonance Studies of a Viscous Nematic Liquid Crystal. *J. Chem. Phys.* **1970**, *52*, 3378−3382.

(33) Pušnik, F.; Schara, M. EPR Study of the Orientational Order and Molecular Dynamics in the Smectic A and Smectic B Phase of a Liquid Crystal. *Chem. Phys. Lett.* **1976**, *37*, 106−109.

DOI: 10.1021/acs.jpcb.9b05431
J. Phys. Chem. B 2019, 123, 5875−5891

(34) Rao, A. S. N.; Murty, P. N.; Murty, C. R. K.; Reddy, T. Rs. EPR Study of Molecular Ordering in Liquid Crystal: NOBA. *Phys. Status Solidi A* **1981**, *68*, 373−377.
(35) Tanaka, H.; Kuwata, K. ESR Study on Molecular Alignment of Various Nitroxides in a Nematic Liquid Crystal. *Bull. Chem. Soc. Jpn.* **1978**, *51*, 2451−2455.
(36) Meirovitch, E.; Luz, Z.; Alexander, S. Magnetic Instabilities of Smectic C Liquid Crystals Studied by Electron Spin Resonance Spectroscopy. *Mol. Phys.* **1979**, *37*, 1489−1507.
(37) Carr, S. G.; Khoo, S. K.; Luckhurst, G. R.; Zannoni, C. On the Ordering Matrix for the Spin Probe (3-spiro [2′-N-oxyl-3′,3′-dimethyloxazolidine])-5α-cholestane, in the Nematic Mesophase of 4,4′-dimethoxyazoxybenzene. *Mol. Cryst. Liq. Cryst.* **1976**, *35*, 7−13.
(38) Imrie, C. T.; Ionescu, D.; Luckhurst, G. R. Molecular Organization of the Polymer Backbone in a Side Group Liquid Crystal Polymer. An ESR Investigation. *Macromolecules* **1997**, *30*, 4597−4600.
(39) Caldeira, J.; Figueirinhas, J. L.; Santos, C.; Godinho, M. H. EPR Spectroscopy of Protein Microcrystals Oriented in a Liquid Crystalline Polymer Medium. *J. Magn. Reson.* **2004**, *170*, 213−219.
(40) Yankova, T. S.; Pomogailo, D. A.; Chumakova, N. A.; Vorobiev, A. Kh. The Novel Stable Nitroxide Radicals as Perspective Spin Probes for Study of Orientation Order of Liquid Crystals and Polymers. *Mol. Cryst. Liq. Cryst.* **2011**, *540*, 196−204.
(41) Yankova, T. S.; Chumakova, N. A.; Pomogailo, D. A.; Vorobiev, A. Kh. Orientational Order of Guest Molecules in Aligned Liquid Crystal as Measured by EPR and UV−VIS Techniques. *Liq. Cryst.* **2013**, *40*, 1135−1145.
(42) Yankova, T. S.; Bobrovsky, A. Yu.; Vorobiev, A. Kh. Order Parameters < P2>, < P4>, and < P6> of Aligned Nematic Liquid-Crystalline Polymer As Determined by Numerical Simulation of Electron Paramagnetic Resonance Spectra. *J. Phys. Chem. B* **2012**, *116*, 6010−6016.
(43) Chumakova, N. A.; Yankova, T. S.; Fairfull-Smith, K. E.; Bottle, S. E.; Vorobiev, A. Kh. Molecular Orientational Order of Nitroxide Radicals in Liquid Crystalline Media. *J. Phys. Chem. B* **2014**, *118*, 5589−5599.
(44) Bogdanov, A. V.; Vorobiev, A. Kh. ESR and Optical Study of Photo-Orientation in Azobenzene-Containing Liquid-Crystalline Polymer. *J. Phys. Chem. B* **2013**, *117*, 12328−12338.
(45) Yankova, T. S.; Chumakova, N. A.; Pomogailo, D. A.; Vorobiev, A. Kh. Spin Probe Orientation Distribution Functions in Aligned Nematic Liquid Crystal. *Magn. Reson. Solids, Electron. J.* **2011**, *13*, 10−13.
(46) Chumakova, N. A.; Vorobiev, A. Kh.; Ikuma, N.; Uchida, Y.; Tamura, R. Magnetic Characteristics and Orientation of a New Nitroxide Radical in an Ordered Matrix. *Mendeleev Commun.* **2008**, *18*, 21−23.
(47) Bogdanov, A. V.; Vorobiev, A. Kh. Orientation Order and Rotation Mobility of Nitroxide Biradicals Determined by Quantitative Simulation of EPR Spectra. *Phys. Chem. Chem. Phys.* **2016**, *18*, 31144−31153.
(48) Freed, J. H. Theory of Slow Tumbling EPR Spectra for Nitroxides. In *Spin Labeling: Theory and Applications*; Berliner, L. J., Ed.; Academic Press: New York, 1976; pp 53−132.
(49) Schneider, D. J.; Freed, J. H. Calculating Slow Motional Magnetic Resonance Spectra. In *Spin Labeling: Theory and Applications*; Berliner, L. J., Reuben, J., Eds.; Plenum Press: New York, 1989; Vol. *8*, pp 1−76.
(50) Budil, D. E.; Lee, S.; Saxena, S.; Freed, J. H. Nonlinear-Least-Squares Analysis of Slow-Motional EPR Spectra in One and Two Dimensions Using a Modified Levenberg−Marquardt Algorithm. *J. Magn. Reson., Ser. A* **1996**, *120*, 155−189.
(51) EasySpin. http://www.easyspin.org/ (accessed April 25, 2019).
(52) Bacchiocchi, C.; Miglioli, I.; Arcioni, A.; Rai, K.; Fontecchio, A.; Zannoni, C. EPR Study of Order and Dynamic of the 5CB Liquid Crystal in an H-PDLC Device. *Mol. Cryst. Liq. Cryst.* **2012**, *558*, 127−139.
(53) Dzikovski, B.; Tipikin, D.; Livshits, V.; Earle, K.; Freed, J. Multifrequency ESR Study of Spin-Labeled Molecules in Inclusion Compounds with Cyclodextrins. *Phys. Chem. Chem. Phys.* **2009**, *11*, 6676−6688.
(54) Pilar, J.; Labsky, J.; Marek, A.; Budil, D. E.; Earle, K. A.; Freed, J. H. Segmental Rotational Diffusion of Spin Labeled Polystyrene in Dilute Toluene Solution by 9 and 250 GHz ESR. *Macromolecules* **2000**, *33*, 4438−4444.
(55) Luckhurst, G. R. On the Creation of Director Disoder in Nematic Liquid Crystals. *Thin Solid Films* **2006**, *509*, 36−48.
(56) Gopee, H.; Cammidge, A. N.; Oganesyan, V. S. Probing Columnar Discotic Liquid Crystals by EPR Spectroscopy with a Rigid-Core Nitroxide Spin Probe. *Angew. Chem.* **2013**, *125*, 9085−9088.
(57) Vecchi, I.; Arcioni, A.; Bacchiocchi, C.; Tiberio, G.; Zanirato, P.; Zannoni, C. Expected and Unexpected Behavior of the Orientational Order and Dynamics Induced by Azobenzene Solutes in a Nematic. *J. Phys. Chem. B* **2007**, *111*, 3355−3362.
(58) Arcioni, A.; Bacchiocchi, C.; Vecchi, I.; Venditti, G.; Zannoni, C. A Comparison of the Effects of Dispersed Hydrophobic or Hydrofilic Aerosil Nanoparticles on the Order and Dynamics of the 5CB Liquid crystal. *Chem. Phys. Lett.* **2004**, *396*, 433−441.
(59) Miglioli, I.; Bacchiocchi, C.; Arcioni, A.; Kohlmeier, A.; Mehl, G. H.; Zannoni, C. Director Configuration in the Twist-Bend Nematic Phase of CB11CB. *J. Mater. Chem. C* **2016**, *4*, 9887−9896.
(60) Bogdanov, A. V.; Proniuk, G. I.; Vorobiev, A. Kh. Magnetic Field Effects in Nematic and Smectic Liquid Crystals Probed by Time Resolved Observation of Orientation Relaxation of the Spin Probe. *Phys. Chem. Chem. Phys.* **2018**, *20*, 18340−18347.
(61) Steinhoff, H.-J.; Hubbell, W. L. Calculation of Electron Paramagnetic Resonance Spectra from Brownian Dynamics Trajectories: Application to Nitroxide Side Chains in Proteins. *Biophys. J.* **1996**, *71*, 2201−2212.
(62) DeSensi, S. C.; Rangel, D. P.; Beth, A. H.; Lybrand, T. P.; Hustedt, E. J. Simulation of Nitroxide Electron Paramagnetic Resonance Spectra form Brownian Trajectories and Molecular Dynamics Simulations. *Biophys. J.* **2008**, *94*, 3798−3809.
(63) Kuprusevicius, E.; Edge, R.; Gopee, H.; Cammidge, A. N.; McInnes, E. J. L.; Wilson, M. R.; Oganesyan, V. S. Prediction of EPR Spectra of Liquid Crystals with Doped Spin Probes from Fully Atomistic Molecular Dynamics Simulations: Exploring Molecular Order and Dynamics at the Phase Transition. *Chem. - Eur. J.* **2010**, *16*, 11558−11562.
(64) Prior, C.; Oganesyan, S. Prediction of EPR Spectra of Lyotropic Liquid Crystals using a Combination of Molecular Dynamics Simulations and the Model-Free Approach. *Chem. - Eur. J.* **2017**, *23*, 13192−13204.
(65) Prior, C.; Danilane, L.; Oganesyan, V. S. All-Atom Molecular Dynamics Simulations of Spin Labeled Double and Single-Strand DNA for EPR Studies. *Phys. Chem. Chem. Phys.* **2018**, *20*, 13461−13472.
(66) Meirovitch, E.; Igner, D.; Igner, E.; Moro, G.; Freed, J. H. Electron-Spin Relaxation and Ordering in Smectic and Supercooled Nematic Liquid Crystals. *J. Chem. Phys.* **1982**, *77*, 3915−3938.
(67) Lange, A.; Marsh, D.; Wassmer, K. H.; Meier, P.; Kothe, G. Electron Spin Resonance Study of Phospholipid Membranes Employing a Comprehensive Line-Shape Model. *Biochemistry* **1985**, *24*, 4383−4392.
(68) Xu, D.; Budil, D. E.; Ober, Ch. K.; Freed, J. H. Rotational Diffusion and Order Parameters of a Liquid Crystalline Polymer Studied by ESR: Molecular Weight Dependence. *J. Phys. Chem.* **1996**, *100*, 15867−15872.
(69) Zerbetto, M.; Polimeno, A.; Cimino, P.; Barone, V. On the Interpretation of Continuous Wave Electron Spin Resonance Spectra of Tempo-Palmitate in 5-Cyanobiphenyl. *J. Chem. Phys.* **2008**, *128*, 024501.
(70) Zerbetto, M.; Polimeno, A.; Barone, V. Simulation of Electron Spin Resonance Spectroscopy in Diverse Environments: An Integrated Approach. *Comput. Phys. Commun.* **2009**, *180*, 2680−2697.

DOI: 10.1021/acs.jpcb.9b05431
J. Phys. Chem. B 2019, 123, 5875−5891

(71) Vorobiev, A. Kh.; Yankova, T. S.; Chumakova, N. A. Orientation Distribution Function and Order Parameters of Oriented Spin Probe as Determined by EPR Spectroscopy. *Chem. Phys.* **2012**, *409*, 61−73.
(72) Polimeno, A.; Freed, J. H. Slow Motional ESR in Complex Fluids: The Slowly Relaxing Local Structure Model of Solvent Cage Effects. *J. Phys. Chem.* **1995**, *99*, 10995−11006.
(73) Sastry, V. S. S.; Polimeno, A.; Crepeau, R. H.; Freed, J. H. Studies of Spin Relaxation and Molecular Dymamics in Liquid Crystals by Two-Dimensional Fourier Transform Electron Spin Resonance. I. Cholestane Butoxy Benzylidene-Octylsniline and Dynemic Cage Effects. *J. Chem. Phys.* **1996**, *105*, 5753.
(74) Van, S. P.; Birrell, G. B.; Griffith, O. H. Rapid Anisotropic Motions of Spin Labels. Models of Averaging of the ESR Parameters. *J. Magn. Reson.* **1974**, *15*, 444−459.
(75) Isaev, N. P.; Kulik, L. V.; Kirilyuk, I. A.; Reznikov, V. A.; Grigor'ev, I. A.; Dzuba, S. A. Fast Stochastic Librations and Slow Small-Angle Rotations of Molecules in Glasses Observed on Nitroxide Spin Probes by Stimulated Electron Spin Echo Spectroscopy. *J. Non-Cryst. Solids* **2010**, *356*, 1037−1042.
(76) Vorobiev, A. Kh.; Gurman, V. S.; Klimenko, T. A. Rotation Mobility of Guest Molecules Studied by Method of Oriented Spin Probe. *Phys. Chem. Chem. Phys.* **2000**, *2*, 379−385.
(77) Timofeev, V.; Samarianov, B. Dynamics of Macromolecule Spin-Labelled Side-Chain Groups by Electron Paramagnetic Resonance Spectra Simulation. *J. Chem. Soc., Perkin Trans. 2* **1995**, 2175−2181.
(78) Vorobiev, A. Kh.; Chumakova, N. A. Simulation of Rigid-Limit and Slow-Motion EPR Spectra for Extraction of Quantitative Dynamic and Orientational Information. In *Nitroxides—Theory, Experiment and Applications*; Kokorin, A. I., Ed.; InTech: Rijeka, Croatia, 2012; pp 58−112.
(79) Dennis, J. E.; Gay, D. M.; Walsh, R. E. An Adaptive Nonlinear Least-Squares Algorithm. *ACM Trans. Math. Software* **1981**, *7*, 348−368.
(80) Seber, G. A. F.; Wild, C. J. *Nonlinear Regression*; Wiley: Hoboken, NJ, 1989.
(81) Dunmur, D. A.; Fukuda, A.; Luckhurst, G. R. *Physical Properties of Liquid Crystals: Nematics*; INSPEC, 2011.
(82) Rojas, E.; Salan, J.; Cesari, E.; Font, J.; Muntasell, J.; Tamarit, J. L. I. Calorimetric Determination of Enthalpy Changes in Octylcyanobiphenyl (8CB) Liquid Crystal Transitions. *Thermochim. Acta* **1987**, *119*, 301−310.
(83) Gunina, M. A.; Kucherepa, N. S.; Pestov, S. M.; Kuz'mina, L. G. Crystal and molecular structure of n-hexyloxyphenyl n-octyloxybenzoate. *Crystallogr. Rep.* **2012**, *57*, 524−527.
(84) Beresnev, L. A.; Blinov, L. M.; Baikalov, V. A.; Pozhidayev, E. P.; Purvanetskas, G. V.; Pavluchenko, A. I. Ferroelectricity in Tilted Smectics Doped with Optically Active Additives. *Mol. Cryst. Liq. Cryst.* **1982**, *89*, 327−338.
(85) Petrov, S.; Simova, P. The Smectic Polymorphism and the Phase Transitions in Liquid Crystal 4, n-Hexyloxyphenyl-4, n'-Decyloxynenzoate. *Cryst. Res. Technol.* **1986**, *21*, 959−965.
(86) Sakagami, S.; Takase, A.; Nakamizo, M.; Kakiyama, H. Microscopic Study on the Molecular Arrangementsin the Smectic A, B and C Modifications. *Mol. Cryst. Liq. Cryst.* **1973**, *19*, 303−313.
(87) Ikuma, N.; Tamura, R.; Shimono, S.; Kawame, N.; Tamada, O.; Sakai, N.; Yamauchi, J.; Yamamoto, Y. Magnetic Properties of All-Organic Liquid Crystals Containing a Chiral Five-Membered Cyclic Nitroxide Unit within the Rigid Core. *Angew. Chem., Int. Ed.* **2004**, *43*, 3677−3682.
(88) Ikuma, N.; Tamura, R.; Shimono, S.; Uchida, Y.; Masaki, K.; Yamauchi, J.; Aoki, Y.; Nohira, H. Ferroelectric Properties of Paramagnetic, All-Organic, Chiral Nitroxyl Radical Liquid Crystals. *Adv. Mater.* **2006**, *18*, 477−480.
(89) Fairfull-Smith, K. E.; Bottle, S. E. The Synthesis and Physical Properties of Novel Polyaromatic Profluorescent Isoindoline Nitroxide Probes. *Eur. J. Org. Chem.* **2008**, *2008*, 5391−5400.
(90) Keddie, D. J.; Fairfull-Smith, K. E.; Bottle, S. E. The Palladium-Catalysed Copper-Free Sonogashira Coupling of Isoindoline Nitroxides: A Convenient Route to Robust Profluorescent Carbon-Carbon Frameworks. *Org. Biomol. Chem.* **2008**, *6*, 3135−3143.
(91) Micallef, A. S.; Blinco, J. P.; George, G. A.; Reid, D. A.; Rizzardo, E.; Thang, S. H.; Bottle, S. E. The Application of a Novel Profluorescent Nitroxide to Monitor Thermo-Oxidative Degradation of Polypropylene. *Polym. Degrad. Stab.* **2005**, *89*, 427−435.
(92) Blinco, J. P.; McMurtrie, J. C.; Bottle, S. E. The First Example of an Azaphenalene Profluorescent Nitroxide. *Eur. J. Org. Chem.* **2007**, *2007*, 4638−4641.
(93) Cecil, R. Model System for Hydrophobic Interactions. *Nature* **1967**, *214*, 369−370.
(94) Soboleva, O. A. Selective Wetting of Heterogeneous Surfaces by Solutions of Surfactants. *Moscow Univ. Chem. Bull.* **2008**, *63*, 9−13.
(95) Pomogailo, D. A.; Paramonov, N. A.; Chumakova, N. A.; Vorobiev, A. Kh. Determination of Relative Positions and Localizations of Paramagnetic Probe Molecules in Liquid Crystal by Analysis of Concentration Broadening of EPR Spectra. *Chem. Phys. Lett.* **2016**, *657*, 53−59.

DOI: 10.1021/acs.jpcb.9b05431
J. Phys. Chem. B 2019, 123, 5875−5891